# Chapter III. Modeling the Effects of Aerosols on Climate

**Author: D. Rind**, NASA GISS, **G. Feingold**, NOAA ESRL; **S. E. Schwartz**, DOE BNL.

## Table of Contents



## 3.1. Introduction

A primary conclusion of the recent IPCC (2007) report is the elevation of man's influence on the warming climate to the category of "very likely". This conclusion is based on among other things the ability of models to simulate the global and to some extent regional variations of temperature over the past 100 years. When anthropogenic effects are included, the simulations can reproduce the observed warming; when they are not, the models do not get very much warming at all. Practically all of the models run for this assessment (approximately 20) produce this distinctive result.

Behind this relative unanimity, however, is an inconvenient truth: in order to produce the observed temperature increase trend, models must use very uncertain aerosol forcing. The greenhouse gas change by itself produces warming in models that exceeds that observed on average by some 40% (IPCC, 2007). Cooling associated with aerosols reduces this warming to the correct level. However, to achieve this response, different climate models use differing aerosol forcings, both direct (aerosol scattering and absorption of short and longwave radiation) and indirect (aerosol effect on cloud cover reflectivity and lifetime), whose magnitudes differ markedly. Kiehl (2007) using nine of the IPCC (2007) AR4 climate models found that they had a factor of three forcing difference in the aerosol contribution for the 20th century. The differing aerosol forcing is the prime reason why models whose climate sensitivity varies by almost a factor of three can produce the 'right' answer. Hence the uncertainty in IPCC (2007) anthropogenic climate simulations for the past 100 years should really be much greater than stated (Schwartz et al., 2007; Kerr, 2007). To clarify this issue, we first review how aerosol radiative forcing is estimated.

### ***3.1.1.*** *Calculating aerosol radiative forcing*

Two different approaches are used to assess the aerosol effect on climate. "Forward modeling" studies incorporate different aerosol types and attempt to explicitly calculate the aerosol radiative forcing. From this approach, IPCC (2007) concluded that the best estimate of aerosol direct radiative forcing (compared with preindustrial times) is –0.5 [±0.4] $Wm^{-2}$, with the contributions as follows: sulfate, –0.4 [±0.2] $Wm^{-2}$; fossil fuel organic carbon, –0.05 [±0.05] $Wm^{-2}$; fossil fuel black carbon, +0.2 [±0.15] $Wm^{-2}$; biomass burning, +0.03 [±0.12] $Wm^{-2}$; nitrate, –0.1 [±0.1] $Wm^{-2}$ ; and mineral dust, –0.1 [±0.2] $Wm^{-2}$. The radiative forcing due to the cloud albedo or brightness effect (also referred to as first indirect or Twomey effect) is estimated to be –0.7 [–1.1, +0.4] $Wm^{-2}$. No estimate was specified for the second indirect effect, associated with cloud lifetime (which was deemed a 'feedback' rather than a forcing). The total negative radiative forcing due to aerosols according to IPCC (2007) estimates is therefore –1.2 $Wm^{-2}$ [range –0.6 to –2]; in contrast the greenhouse warming (including tropospheric ozone) is estimated to be about 3 $Wm^{-2}$, hence tropospheric aerosols reduce this influence by 40% [20-80%].

The other method of calculating aerosol forcing is called the 'inverse approach' – it is assumed that the observed climate change is primarily the result of the known climate forcing contributions. If one assumes a climate sensitivity (or a range of sensitivities), one can determine what the total forcing had to be to produce the observed temperature change. The aerosol forcing is then deduced as a residual after subtraction of the GHG forcing along with other known forcings from the total value. Studies of this nature come up with aerosol forcing ranges of –0.6 to –1.7 $Wm^{-2}$ (Knutti et al., 2002, 2003; IPCC Chap.9); -0.4 to –1.6 $Wm^{-2}$ (Gregory et al., 2002); and -0.4 to –1.4 $Wm^{-2}$ (Stott **et al**., 2006).

Anderson et al. (2003) reviewing the full magnitude of "forward modeling" studies noted that the results showed a much wider range than appears in the IPCC report, with negative values as large as –4 $Wm^{-2}$, obviously outside of the range of the inverse estimates. They concluded that either these more extreme forward calculations are incorrect, or natural variability is being underestimated, or climate sensitivity is much larger than anticipated. We return to this discussion in section 3.4. Next we review how the modeling of aerosol radiative forcing for the IPCC AR4 report was carried out.

### ***3.1.2.*** *Modeling aerosol direct radiative forcing*

In the prescribed climate modeling simulations conducted for the IPCC (2007) AR4 report, a scenario of aerosol sulfur concentrations in the atmosphere was made available to the different modeling groups. It used the historical reconstruction of sulfur emissions by Lefohn et al. (1999) rescaled to the SRES (1990) [Special Report on Emission Scenarios, prepared for IPCC, 1990] values to avoid discontinuities with future climate projections. The sources were then run in the French LMD chemical transport and transformation model to produce column average aerosol distributions over the globe (Boucher and Pham, 2002). At least four GCMs employed this distribution, although it was not mandatory, and many did not, preferring their own approaches. The global sulfur emission estimates from different studies are well constrained, with seven different reconstructions of sulfur emissions having a standard deviation of less than 20% among them for the time period between 1890 and 1990 (IPCC, 2007). However, the modeling groups which didn't use the Boucher and Pham distribution had to convert time-dependent sulfur emissions to regionally dependent sulfate concentrations and optical depth, and the techniques used were model-dependent. For example, NCAR incorporated historical $SO_2$ emissions from the data set of Smith et al. (2001) into the MOZART global chemical transport model to produce its sulfate distribution. GFDL also used MOZART with time-varying aerosols. GISS used time-varying aerosols in a version of the full GCM that included additional aerosol-related processes, with the distributions saved for use in the climate-change simulations. As will be shown, the varying procedures resulted in varying sulfate concentrations. And as the models also use different aerosol radiative characteristics along with differing atmospheric radiation schemes, the subsequent radiative forcing is even more model-dependent.

As an illustration of the uncertainty to be found, shown in **Table 3.1** are the various global sulfate aerosol loads, optical depths and direct radiative forcings relative to preindustrial times in aerosol and climate models published since the Third Annual IPCC report (TAR) {adapted from IPCC 2007, Table 2.4} (see Section 1 for the distinction between aerosol models and climate models). These may be thought of as the "extensive" properties of the aerosols. Also indicated (in the last three columns) are the "intensive" properties, the mass scattering efficiency, forcing per optical depth, and forcing relative to the mass of aerosol ("normalized forcing"). While the amount of aerosol may be considered a product of the model's sources and sinks ('extensive influences) which influence its optical depth, the efficiency with which an aerosol scatters (i.e., the intensity) translates this aerosol loading into radiative forcing. Considerable variation exists in each of these quantities, with the standard deviation about 40% of the average radiative forcing. Note that the range shown in the table does not necessarily indicate the range in the IPCC climate change experiments, but is indicative of the level of understanding during the time the IPCC AR4 simulations were being carried out. A more direct comparison between several of the GCMs used for the 20$^{th}$ century climate change experiments is provided in Section 3.2.

Note the following model abbreviations for this and similar tables:
CCM3: Community Climate Model; GEOSCHEM: Goddard Earth Observing System-Chemistry; GISS: Goddard Institute for Space Studies; SPRINTARS: Spectral Radiation-Transport Model for Aerosol Species; LMD: Laboratoire de Meteorologie Dynamique; LOA: Laboratoire d'Optique Atmospherique; GATORG: Gas, Aerosol Transport and General circulation model; PNNL: Pacific Northwest National Laboratory; UIO-CTM: Univeristy of Oslo CTM; UIO-GCM: University of Oslo

**Table 3.1.** Sulfate load, optical depth and radiative all-sky forcing in different models. For model designation and appropriate references, see IPCC, 2007, Table 2.4, from which this was adapted. Note that the different GISS model results arise from different aerosol physics packages.

| # Model | Sulfate load (mg $m^{-2}$) | Optical Depth (0.55 μm) | Radiative Forcing ($Wm^{-2}$) | Mass scat. efficiency $m^2 g^{-1}$ | Forcing per Opt. Depth $W m^{-2}$ | Normalized forcing $W g^{-1}$ |
|---|---|---|---|---|---|---|
| *PUBLISHED SINCE IPCC, 2001* | | | | | | |
| A CCM3 | 2.23 | | -0.56 | | | -251 |
| B GEOSCHEM | 1.53 | 0.018 | -0.33 | 11.8 | -18 | -216 |
| C GISS | 3.3 | 0.022 | -0.65 | 6.7 | -30 | -197 |
| D GISS | 3.27 | | -0.96 | | | -294 |
| E GISS* | 2.12 | | -0.57 | | | -269 |
| F SPRINTARS | 1.55 | 0.015 | -0.21 | | | -135 |
| G LMD | 2.76 | | -0.42 | | | -152 |
| H LOA | 3.03 | 0.03 | -0.41 | 9.9 | -14 | -135 |
| I GATORG | 3.06 | | -0.32 | | | -105 |
| J PNNL | 5.5 | 0.042 | -0.44 | 7.6 | -10 | -80 |
| K UIO-CTM | 1.79 | 0.019 | -0.37 | 10.6 | -19 | -207 |
| L UIO-GCM | 2.28 | | -0.29 | | | -127 |
| *AEROCOM (different models used identical emissions)* | | | | | | |
| M UMI | 2.64 | 0.02 | -0.58 | 7.6 | -29 | -220 |
| N UIO-CTM | 1.7 | 0.019 | -0.36 | 11.2 | -19 | -212 |
| O LOA | 3.64 | 0.035 | -0.49 | 9.6 | -14 | -135 |
| P LSCE | 3.01 | 0.023 | -0.42 | 7.6 | -18 | -140 |
| Q ECHAM5-HAM | 2.47 | 0.016 | -0.46 | 6.5 | -29 | -186 |
| R GISS** | 1.34 | 0.006 | -0.19 | 4.5 | -32 | -142 |
| S UIO-GCM | 1.72 | 0.012 | -0.25 | 7.0 | -21 | -145 |
| T SPRINTARS | 1.19 | 0.013 | -0.16 | 10.9 | -12 | -134 |
| U ULAC | 1.62 | 0.02 | -0.22 | 12.3 | -11 | -136 |
| **Average A-L** | **2.8** | **0.024** | **-0.46** | **9.3** | **-18** | **-181** |
| **Average M-U** | **2.15** | **0.018** | **-0.35** | **8.6** | **-21** | **-161** |
| **Minimum A-U** | **1.19** | **0.006** | **-0.96** | **4.5** | **-10** | **-80** |
| **Maximum A-U** | **5.50** | **0.042** | **-0.16** | **12.3** | **-32** | **-294** |
| **rel std dev A-L** | **0.40** | **0.41** | **0.44** | **0.23** | **0.40** | **0.38** |
| **rel std dev M-U** | **0.39** | **0.45** | **0.43** | **0.30** | **0.37** | **0.22** |

*Note that the the aerosol scheme used in this version of the GCM is totally different than that in the GISS climate model discussed below.

** The AEROCOM GISS model uses totally different sources than were used for the historic simulations.

GCM; UMI: University of Michigan; LSCE: Laboratoire des Sciences du Climat et de l'Enviornment; ECHAMS5-HAM: European Centre Hamburg with Hamburg Aerosol Module; ULAQ: University of lL'Aquila.

As expected the relative standard deviations of the intensive properties were somewhat lower than those of the extensive variables, but of comparable magnitude and therefore contributing substantially to the variance in the total radiative forcing. The extensive and intensive properties of the several models are compared in **Figure 3.1**. It is seen that there can be substantial variation in intensive variables, and that even for models that exhibit similar normalized forcing, there can be compensation between mass scattering efficiency and forcing per optical depth.

The values (and relative standard deviations, RSDs) of mass scattering efficiency and normalized forcing have been examined in an intercomparison of radiative transfer models (Boucher et al, 1998). That study showed that for a well specified aerosol (size, composition, relative humidity) the mass scattering

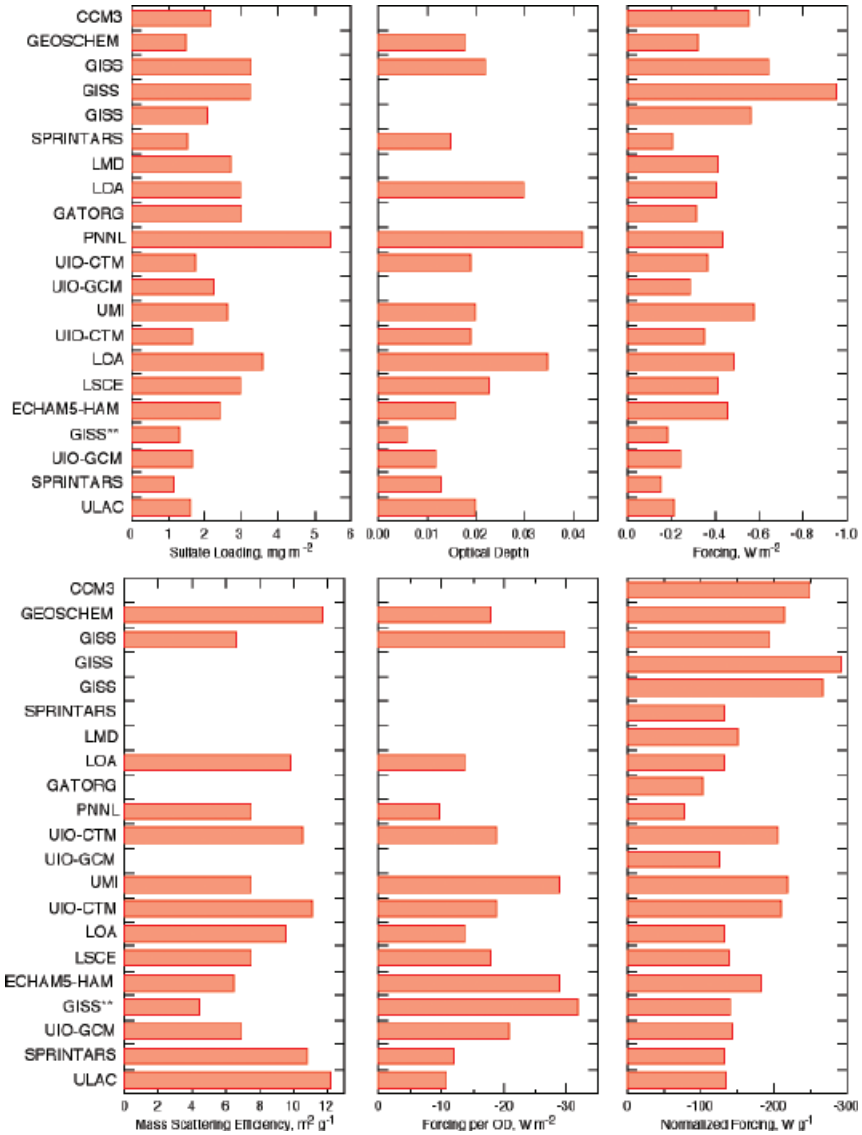


**Figure 3.1** Extensive (top) and intensive (bottom) aerosol properties of models in Table 3.1. Note that scales of negative quantities are reversed so that the magnitudes of all plotted quantities increase to the right.

efficiency as determined by the several models agrees quite precisely (**Figure 3.2**, left). The rather low values of mass scattering efficiency by the several GCMs ( < 9 $m^2$ $g^{-1}$) (**Figure 3.1**) suggests that the particle radii were all considerably lower than the mode radius 0.33 μm, a radius value that would give a much greater mass scattering efficiency of about 20 $m^2$ $g^{-1}$. The spread in GCM mass scattering efficiency (27% RSD) is likely due to the spread in the size distributions assumed or calculated in the several models, which could arise from both the intrinsic size distribution and the environmental relative humidity experienced by the aerosols in the different models.

For the radiative transfer calculations leading to determination of normalized forcing in the model intercomparison of Boucher et al. (1998), the atmospheric conditions (relative humidity profile) and surface reflectance were also quite well specified, resulting in a RSD of 8% in normalized forcing at the particle radius corresponding to the greatest normalized forcing (**Figure 3.2**, right). The much greater spread in this quantity for the GCMs examined in Table 3.1 (33% RSD) would appear more a consequence of variations in aerosol properties (cf. the 27% RSD in mass scattering efficiency) than of differences in the radiative transfer algorithms. The mode radius of the sulfate particles inferred from the normalized forcing is considerably less than that inferred from the mass scattering efficiency; the reason for this is not known.

In summary, the differences among models in the direct radiative effect of sulfate aerosols appear to be associated primarily with different magnitudes of sulfate loading, different size distributions of the sulfate aerosol, and different relative humidity influences. Ideally, these are all aspects which should be able to be constrained by observations, if not now then with continuing research.

For the other aerosol constituents, the climate modelers used perhaps even more diverse approaches, in part because the historical variation with time of other aerosol sources is less well-known. For example, the NCAR group scaled their current black and organic carbonaceous aerosols from present-day to earlier years using a global scaling for population.  The GISS group used time-and spatially-varying emis-

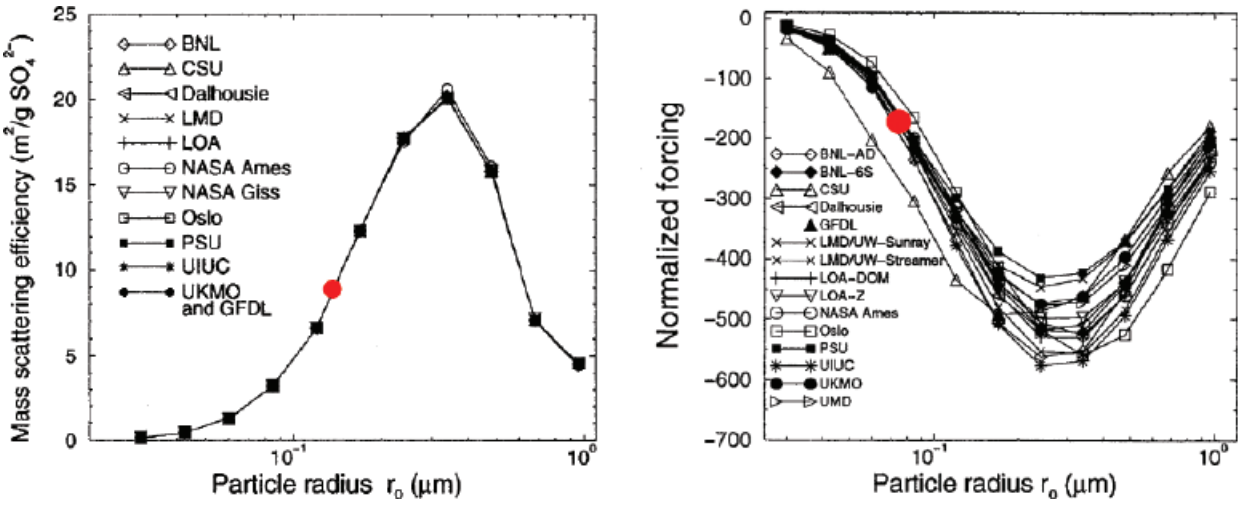


**Fig 3.2.** Mass scattering efficiency (left) and global-average normalized forcing (forcing per sulfate loading, W m-2 /(g m-2) or W g-1) (right) as evaluated by 15 radiation transfer models for a well specified aerosol (ammonium sulfate at 80% relative humidity) and well specified surface albedo, as a function of particle radius. (Boucher et al., 1998). Red circles denote ordinate values corresponding to averages of models in Table 3.1.

sions based on fuel use, but then normalized the black carbon (BC) and organic carbon (OC) amounts to obtain best correspondence with the present day with AERONET data (Hansen et al., 2007). GFDL ran MOZART simulations two years every decade from 1869-2000 with varying emissions [historical emissions produced by scaling present-day values based on the EDGAR-HYDE historical emissions inventory (Van Ardenne et al., 2001)] but the same present-day wind fields, with year-to-year variations imposed by linear interpolation. As with sulfate, further differences arose because of the use of differing aerosol optical characteristics and differing radiation schemes.

**Table 3.2:** As in Table 3.1 for the carbonaceous aerosols: particulate organic matter (POM) and black carbon (BC). From IPCC 2007 Table 2.5.

| # Model | POM LOAD (mg POM $m^{-2}$) | POM Optical Depth (0.55μm) | POM Radiative Forcing ($Wm^{-2}$) | mass scat effic, $m^2$ $g^{-1}$ | forcing per OD, W $m^{-2}$ OD-1 | Normalized forcing, W/g | BC LOAD (mg BC $m^{-2}$) | BC RAD. FORCING ($Wm^{-2}$) | Normalized forcing, W/g |
|---|---|---|---|---|---|---|---|---|---|
| *PUBLISHED SINCE IPCC, 2001* | | | | | | | | | |
| A SPRINTARS | | | -0.24 | | | | | 0.36 | |
| B LOA | 2.33 | 0.016 | -0.25 | 6.9 | -16 | -107 | 0.37 | 0.55 | 1486 |
| C GISS | 1.86 | 0.017 | -0.26 | 9.1 | -15 | -140 | 0.29 | 0.61 | 2103 |
| D GISS | 1.86 | 0.015 | -0.3 | 8.1 | -20 | -161 | 0.29 | 0.35 | 1207 |
| E GISS | 2.39 | | -0.18 | | | -75 | 0.39 | 0.5 | 1282 |
| F GISS | 2.49 | | -0.23 | | | -92 | 0.43 | 0.53 | 1233 |
| G SPRINTARS | 2.67 | 0.029 | -0.27 | 10.9 | -9 | -101 | 0.53 | 0.42 | 792 |
| H GATORG | 2.56 | | -0.06 | 0.0 | | -23 | 0.39 | 0.55 | 1410 |
| I MOZGN | 3.03 | 0.018 | -0.34 | 5.9 | -19 | -112 | | | |
| J CCM | | | | | | | 0.33 | 0.34 | 1030 |
| K UIO-GCM | | | | | | | 0.3 | 0.19 | 633 |
| *AEROCOM (different models used identical emissions)* | | | | | | | | | |
| L UMI | 1.16 | 0.006 | -0.23 | 5.2 | -38 | -198 | 0.19 | 0.25 | 1316 |
| M UIO-CTM | 1.12 | 0.0058 | -0.16 | 5.2 | -28 | -143 | 0.19 | 0.22 | 1158 |
| N LOA | 1.41 | 0.0085 | -0.16 | 6.0 | -19 | -113 | 0.25 | 0.32 | 1280 |
| O LSCE | 1.5 | 0.0079 | -0.17 | 5.3 | -22 | -113 | 0.25 | 0.3 | 1200 |
| P ECHAM5-HAM | 1 | 0.0077 | -0.01 | 7.7 | -1 | -10 | 0.16 | 0.2 | 1250 |
| Q GISS | 1.22 | 0.006 | -0.14 | 4.9 | -23 | -115 | 0.24 | 0.22 | 917 |
| R UIO-GCM | 0.88 | 0.0045 | -0.06 | 5.1 | -13 | -68 | 0.19 | 0.36 | 1895 |
| S SPRINTARS | 1.84 | 0.02 | -0.1 | 10.9 | -5 | -54 | 0.37 | 0.32 | 865 |
| T ULAC | 1.71 | 0.0075 | -0.09 | 4.4 | -12 | -53 | 0.38 | 0.08 | 211 |
| **Average A-K** | **2.38** | **0.019** | **-0.24** | | | | **0.38** | **0.44** | |
| **Average L-T** | **1.32** | **0.008** | **-0.13** | | | | **0.35** | **0.25** | |
| Average A-T | 1.83 | 0.012 | -0.18 | 5.6 | -17 | -99 | 0.31 | 0.35 | 1182 |
| **Average A-T** | **0.42** | **0.006** | **0.08** | | | | **0.08** | **0.13** | |
| **Std. Dev. L-T** | **0.32** | **0.005** | **0.05** | | | | **0.08** | **0.08** | |
| Rel Std Dev A-T | 0.36 | 0.60 | 0.53 | 0.43 | 0.54 | 0.49 | 0.32 | 0.42 | 0.36 |
| **Expected** | | | 0.61 | | | | | 0.49 | |

Again, as an illustration of present uncertainty, shown in **Table 3.2** {from IPCC 2007, Table 2.5} are estimates of anthropogenic carbonaceous aerosol forcing from aerosol and climate models published since the TAR. Organic carbon forcing ranges from –0.06 to –0.34 $Wm^{-2}$ whereas black carbon values range from 0.08 to 0.61 $Wm^{-2}$; relative standard deviations among the models are about 30% in both cases. As was true for sulfate aerosols, the relative standard deviations of the intensive variables are as large or larger than those of the extensive variables and with rather extreme outlier values.

Additionally, even the choice of which aerosols to incorporate was left open to the modelers. Presented in **Table 3.3** {adapted from SAP 1.1 Table 5.2} are the time-varying aerosol forcings employed in the different climate model simulations of the last 100 years for IPCC AR4. As can be seen, all the climate models used a sulfate aerosol direct effect, while fewer than half incorporated a sulfate aerosol indirect forcing; about half used black carbon and organic carbon forcing; and about a quarter used mineral dust and sea salt (which should not generally affect anthropogenic forcing differences).

### ***3.1.3*** *Modeling the aerosol indirect effect*

Whether modelers incorporated an indirect aerosol cloud forcing was also left up to them, and as noted fewer than half the groups incorporated such forcing for sulfates. Shown in **Figure 3.3** {from IPCC 2007 Fig. 2.14} are results from published model studies indicating the different radiative forcing values from the first indirect effect (cloud albedo). This cloud albedo effect ranges from –0.22 to –1.85 $Wm^{-2}$; the lowest estimates of the derivations from simulations that constrained representation

| | MODEL | G | O | SD | SI | BC | OC | MD | SS |
|---|---|---|---|---|---|---|---|---|---|
| 1 | CCCma-CGCM3.1(T47) | | | | | | | | |
| 2 | CCSM3 | | | | | | | | |
| 3 | CNRM-CM3 | | | | | | | | |
| 4 | CSIRO-Mk3.0 | | | | | | | | |
| 5 | ECHAM5/MPI-OM | | | | | | | | |
| 6 | FGOALS-g1.0 | | | | | | | | |
| 7 | GFDL-CM2.0 | | | | | | | | |
| 8 | GFDL-CM2.1 | | | | | | | | |
| 9 | GISS-AOM | | | | | | | | |
| 10 | GISS-EH | | | | | | | | |
| 11 | GISS-ER | | | | | | | | |
| 12 | INM-CM3.0 | | | | | | | | |
| 13 | IPSL-CM4 | | | | | | | | |
| 14 | MIROC3.2(medres) | | | | | | | | |
| 15 | MIROC3.2(hires) | | | | | | | | |
| 16 | MRI-CGCM2.3.2 | | | | | | | | |
| 17 | PCM | | | | | | | | |
| 18 | UKMO-HadCM3 | | | | | | | | |
| 19 | UKMO-HadGEM1 | | | | | | | | |

**Table 3.3** Greenhouse gas and tropospheric aerosol forcings used in IPCC simulations of 20th century climate change. Forcings used are: well-mixed greenhouse gases (G), tropospheric and stratospheric ozone (O), sulfate aerosol direct (SD) and indirect effects (SI), black carbon (BC) and organic carbon aerosols (OC), mineral dust (MD), and sea salt (SS). Adapted from IPCC 1.1, Table 5.2.

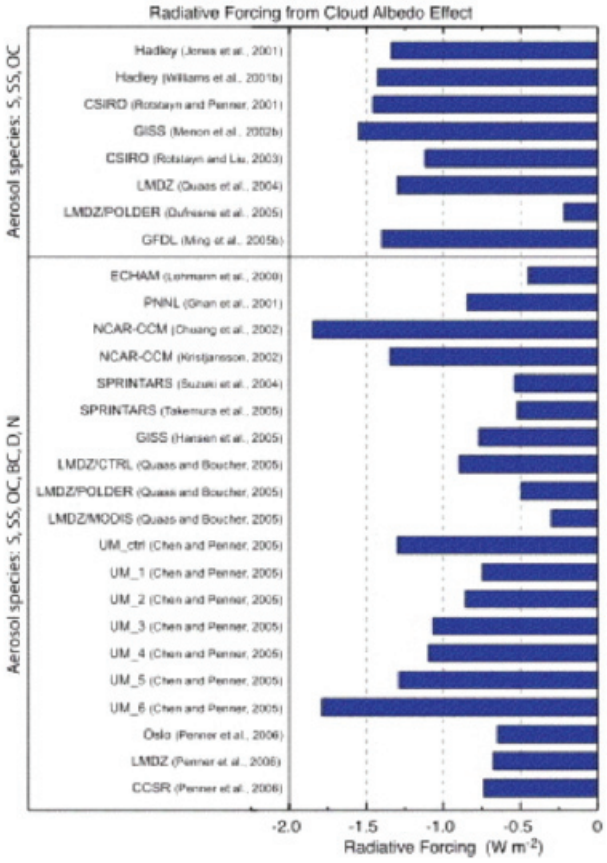


**Fig. 3.3.** Radiative forcing from the cloud albedo effect (1st aerosol indirect effect) in the global climate models used in IPCC 2007 (IPCC Fig. 2.14). For additional model designations and references, see IPCC 2007, chapter 2.

of aerosol effects on clouds with satellite measurements. In view of the difficulty of quantifying this effect remotely, it is not clear whether this constraint provides an improved estimate.

[In the following figure, species included in the lower part of the panel include sulfate, sea salt, organic and back carbon, dust and nitrates; in the top panel only sulfate, sea salt and organic carbon.]

Most models do not incorporate the second indirect effect (on cloud lifetimes, due to the alteration in cloud droplet sizes and precipitation efficiency). However, Hansen et al. (2007) argue that the effect can be substantial; in that study, it was estimated that increased cloud lifetimes (rather than cloud brightness) could help in producing the 'required' –1.2 $Wm^{-2}$. Models in general do not agree on the relative importance of the albedo and lifetime effects. For example, the ratio of second to first indirect effects ranges from about 0.2 to 1.4 in the models reviewed by Lohmann and Feichter (2005). Differences in models are likely related to the aerosol microphysical parameterizations employed, as well as to assumptions about the aerosol background.

It is obvious that modelers have used quite different approaches to produce the aerosol forcing that has resulted in bringing model simulations into line with observations. As noted by Kiehl (2007), the aerosol cooling has been greater in models with larger climate sensitivity. Most of these simulations were conducted several years ago, in time for the IPCC (2007) report. Since then there have been additional studies comparing aerosol observations with what the climate models actually used. In the next section we review the results of those studies, and examine the implications for the ability of models to reproduce the climate record of the last century.

## 3.2. Comparison of Aerosol Direct Effect in Observations and GCMs

Several comparisons have been made between observations and the aerosols used in GCMs. We will discuss two United States models in detail, from the Goddard Institute for Space Studies (GISS) and the Geophysical Fluid Dynamics Laboratory (GFDL). The purpose in presenting these comparisons is to help elucidate how modelers go about assessing their aerosol components, and the difficulties that entails. Here we are concerned with the aerosols that were actually used in the climate model experiments for AR4. Comparisons with observations have already led to some improvements that can be implemented in climate models for subsequent climate change experiments (e.g., Koch et al., 2006). This aspect is discussed further in chapter 4.

The three parameters that define the aerosol radiative forcing are the aerosol optical depth, the single scattering albedo [at the reference wavelength of 0.55 μm] and the phase function or asymmetry factor (all of which are wavelength dependent). The aerosol optical depth ($\tau$) is indicative of how much aerosol exists in the column, and specifically relates to the magnitude of interaction between the aerosols and short- or longwave radiation. The greater the optical depth, the greater the interaction, and for shortwave (solar) radiation and reflective aerosols, that results in greater cooling. The single scattering albedo ($\varpi$) indicates the degree of short or long wave absorption versus the fraction of optical depletion that is due to scattering rather than absorption. The higher the value of $\varpi$, the smaller the absorption, and again for solar radiation, the greater the cooling for the planet as a whole. The phase function or asymmetry factor relates to the angle of scattering; when the scattering is primarily backward, solar radiation is reflected out toward space and cooling predominates. This last aspect is related to the size of the particles; for bigger particles, relative to the wavelength of the light being scattered, more radiation is scattered forward, and hence cooling is reduced. An indication of the particle size is provided by another parameter, the Ångstrom exponent (Å), which is a measure of wavelength dependence; for typical tropospheric aerosols, the Ångstrom exponent for scattering tends to be inversely dependent on particle size; up to a certain point, larger values of Å are thus associated with smaller aerosols and greater cooling. These parameters are further related; for example, for a given composition, the ability of a particle to scatter radiation decreases more rapidly with decreasing size than does its ability to absorb, so models at a given wavelength can vary $\varpi$ by varying Å. In the following sub-section, we review the realism of these features in the GISS model to illustrate more precisely the impact of modeling choices.

### ***3.2.1.*** *The GISS Model*

The aerosols and aerosol forcing in the GISS model have been assessed by Liu et al. (2006). The GISS aerosol climatology is obtained from chemistry-transport model simulations that produce monthly mean height distributions of aerosol mass densities at each grid box (Koch, 2001). The spatial distributions of sulfate, sea salt, nitrate, dust, black carbon and organic carbon aerosols are described in Schmidt et al. (2006), and in greater detail by Liu et al. (2006).

Aerosol optical depth can be related to aerosol mass loading as

$$\tau = \frac{3Q_{ext}M}{4\pi\rho r_{eff}}$$

where M is the aerosol mass loading per unit area, $Q_{ext}$ is the extinction efficiency factor (related to the phase function and single scattering albedo), $r_{eff}$ is the effective radius (related to the particle size distribution and hence Ångstrom coefficient), and $\rho$ is the specific density of the aerosol. This relationship is a simplification for the relatively large particles that contribute appreciably to mass concentration (a full derivation is included as Appendix A.1). Note that the particle size, density and extinction coefficient implicitly vary with height, due to variations in both their concentration and relative humidity, which influences these characteristics.

Therefore, to convert the aerosol mass loadings to optical properties, the size distribution and phase functions must be assigned. Dry size effective radii are specified for each of the aerosol types, and laboratory-measured phase functions are employed for all solar and thermal wavelengths [see the list of references in Liu et al. (2006); be advised, however, that questions remain concerning the pertinence of laboratory-determined refractive indices for the organic carbon and black carbon that exist in the atmosphere where, as but one example, internal mixtures can influence the refractive properties.] With these specifications, the optical thickness and scattering optical properties of the various aerosols are defined for the somewhat arbitrarily specified (dry) particle sizes. In addition, for hygroscopic aerosols (sulfate, nitrate, sea salt and organic carbon), formulas are used for the particle growth of each aerosol as a function of relative humidity, including the change in density and refractive index. In practice, look-up tables for extinction coefficients (i.e., aerosol refractive properties) as a function of relative humidity are employed based on laboratory measurements [see Schmidt et al., 2006 for details, but again the accuracy of these measurements is not fully established. The field observations discussed in Chapter 2 provide a reality check.] While the aerosol distribution is prescribed as monthly mean values, the relative humidity component of the extinction is updated each hour.

The GISS climate model aerosol distribution and properties used for 1990 and subsequent years is compared with satellite data sets from MODIS (the particular version used is referred to as "collection 4 data without deep blue retrieval over deserts"), MISR, POLDER and AVHRR, with additional data from TOMS and ground-based measurements (AERONET). The GISS climate model does not vary its aerosols after 1990, so comparisons with satellite retrievals after that date are all being made with the same model values. The GCM comparisons are for cloud-free conditions, theoretically consistent with the satellite aerosol retrievals being used (although determination of when a cloud is present by satellite is not always unequivocal); the GISS model has either cloud-free or cloud-covered grid boxes at each point in time (there is no partial cloud cover), and thus there is no ambiguity for the model in this regard. Satellite measurements are also subject to errors arising from both measurement uncertainty and assumptions in converting from radiance to optical depth.

Here, following Liu et al. (2006), we compare modeled and observed aerosol characteristics. Shown in **Figure 3.4 a,b** (adapted from Liu et al., 2006 Fig. 1a,b) are the global optical depth distributions of aerosols from the GISS model along with the various observational data sets for the two solstice seasons. Qualitative agreement is apparent, with generally higher burdens in Northern Hemisphere summer, and seasonal variations of smoke over southern Africa and South America, as well as wind blown dust over northern African and the Persian Gulf. Aerosol optical depth in both model and observations is smaller away from land. Note that there are differences among the observational data sets themselves, due at least in part to characteristics of the retrievals. For example, over land, POLDER retrieves aerosol properties only in the accumulation mode (i.e., small aerosols). Disagreement among observational data sets obviously makes model validation more difficult.

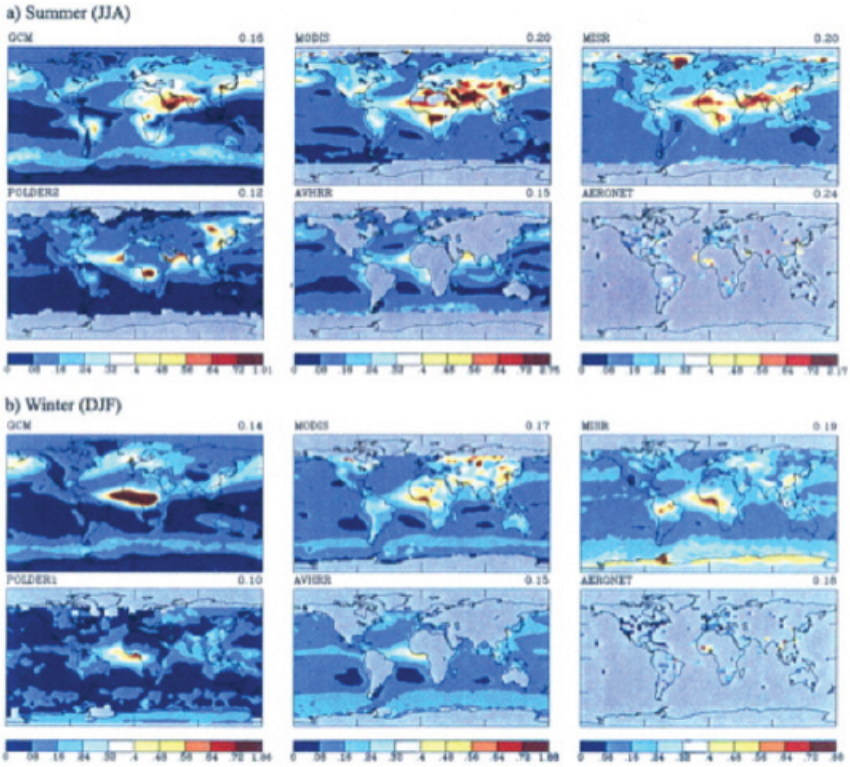


**Fig. 3.4.** GISS climate model aerosol optical depth at 0.55 μm in June-August (a) and December-February (b) compared with satellite observations (MODIS, MISR, POLDER and AVHRR) as well as surface-based observations (AERONET). Note all satellite comparisons presented are for clear-sky conditions. From Liu et al. (2006).

These comparisons include both natural and anthropogenic aerosols. Errors in modeling natural aerosols do not necessarily affect calculations of the direct aerosol influence on climate change, at least to first order, but they do affect the assessment of the anthropogenic component of the total aerosol characteristics.

There are, however, considerable discrepancies between the model and observations. Overall, the GISS GCM has reduced aerosol optical depths compared with the satellite data (a global, clear-sky average of about 80% compared with MODIS and MISR data), although it is in better agreement with AERONET ground-based measurements in some locations (note that the input aerosol values were

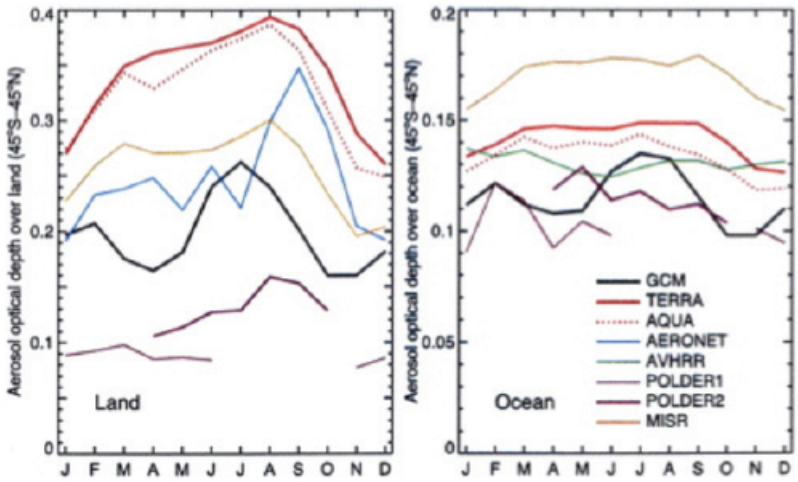


**Fig. 3.5.** Seasonal dependence of the area weighted monthly mean aerosol optical depth in the GISS climate model (GCM) and observational data sets. From Liu et al. (2006).

calibrated with AERONET data). The model values over the Sahel in Northern Hemisphere winter and the Amazon in Southern Hemisphere winter are excessive, indicative of errors in the biomass burning distributions, at least partially associated with an older biomass burning source estimate (the source used here was from Liousse et al., 1996).

The seasonal distribution of the aerosol optical depth is shown in **Figure 3.5** {adapted from Liu et al., 2006, Fig. 4} (the legends "Terra" and "Aqua" refer to the MODIS instruments on board each of these satellites). While the absolute value of the differences are as large among the observations themselves as they are between the GISS model and some observations, the seasonal dependence in the GISS

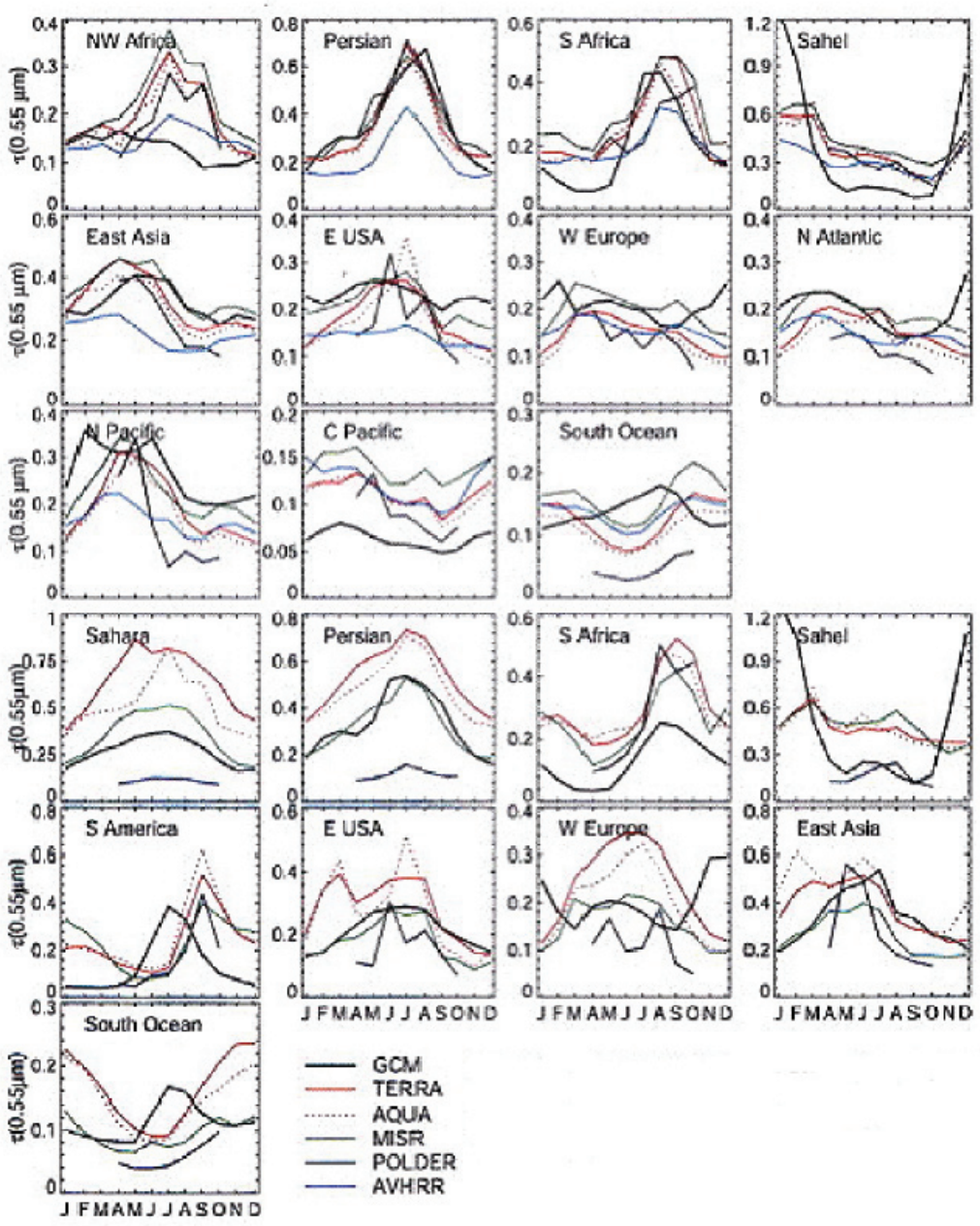


**Fig. 3.6.** Regional analysis of the monthly mean aerosol optical depth at 0.55 μm in the GISS GCM and from observations, over water surfaces (top three rows) and over land (bottom three rows). From Liu et al., (2006).

model appears different, with, for example, spring and fall minima in optical depth that is not seen in observations.

Because of the heterogeneous nature of its forcing, aerosol impacts are often viewed in terms of their geographical influence on radiation and temperature. Shown in **Figure 3.6** {adapted from Liu et al., 2006 Fig. 7} is a regional comparison of the optical depths as a function of month. Despite the global-average mismatch, the model seasonal variation is in qualitative agreement with the observations for many of these locations, all of which represent major aerosol regimes. The relative contributions of the different aerosol types to the optical depth in these regions is given in **Figure 3.7** {adapted from Liu

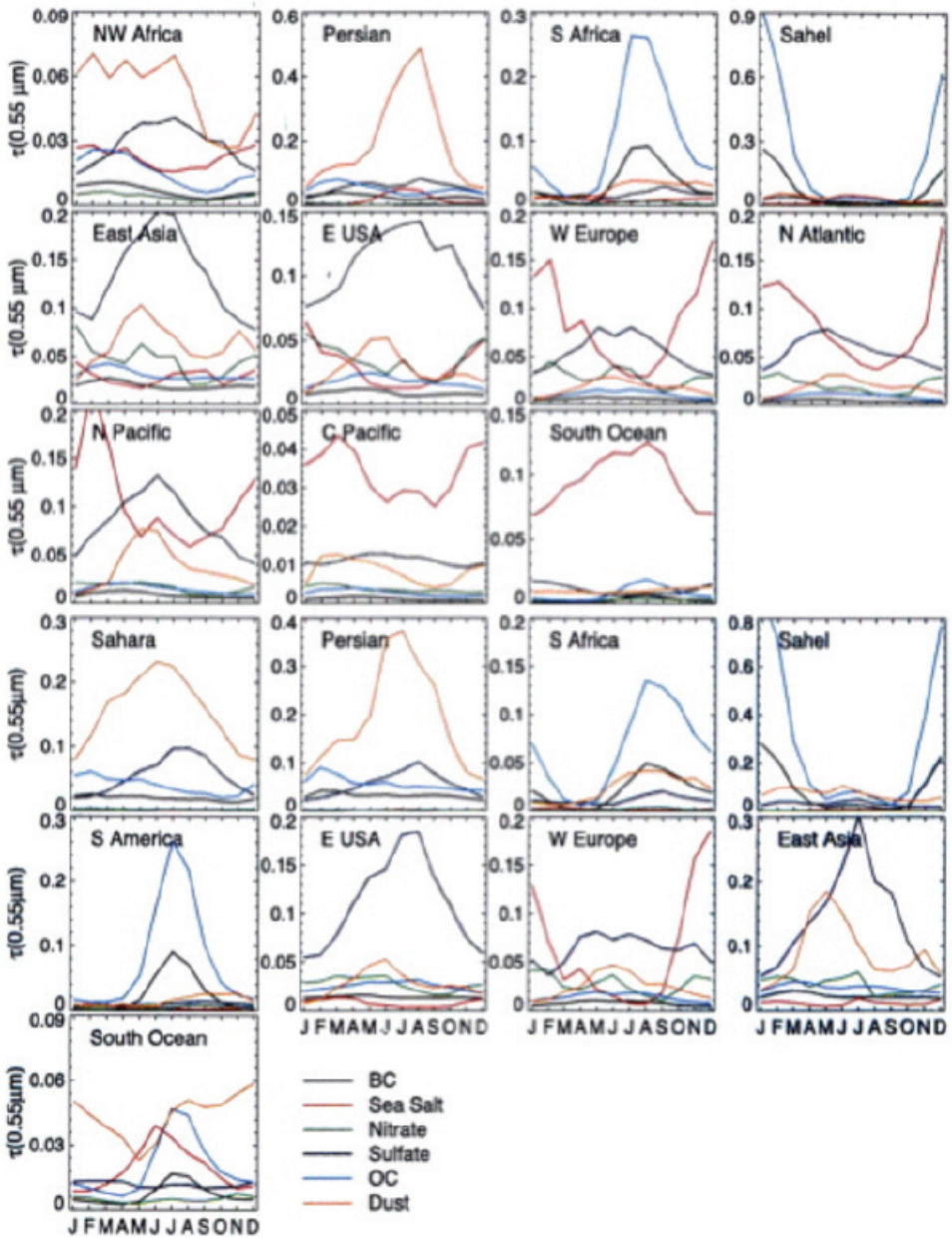


**Fig. 3.7.** Contributions of each aerosol component in the GCM to the total optical depth at 0.55 μm in the various regions. From Liu et al. (2006).

et al., 2006 Fig. 8}. In combination with **Figure 3.6** one can see that the higher model values in the Sahel during January are due to organic carbon aerosols from biomass burning. A primary discrepancy in the seasonal cycle occurs in the Southern Hemisphere ocean region (30°S-60°S) where the model shows a maximum in austral winter, opposite to what appears in the observations. Given that winds are strongest in winter, one would expect the sea salt concentration to be maximum at that time, as in the model parameterization; potential cloud cover contamination in this region may be influencing the observations from all the satellite data sets. Nevertheless, as shown by Koch et al. (2006), this model has excessive sea salt aerosols in the Southern Ocean. In addition, the seasonal variation may actually be controlled by sulfate from DMS oxidation and biomass burning transported from southern Africa and South America, hence the opposite model seasonal cycle may be also be associated with problems due to these sources. Determining the reason for model/data mismatches requires multiple experiments and various types of observations.

The Ångstrom exponent in the model and observations is shown in **Figure 3.8** {adapted from Liu et al., 2006, Fig. 2a,b}. This parameter is important because the particle size distribution affects the efficiency of scattering of both short and longwave radiation, as discussed earlier.

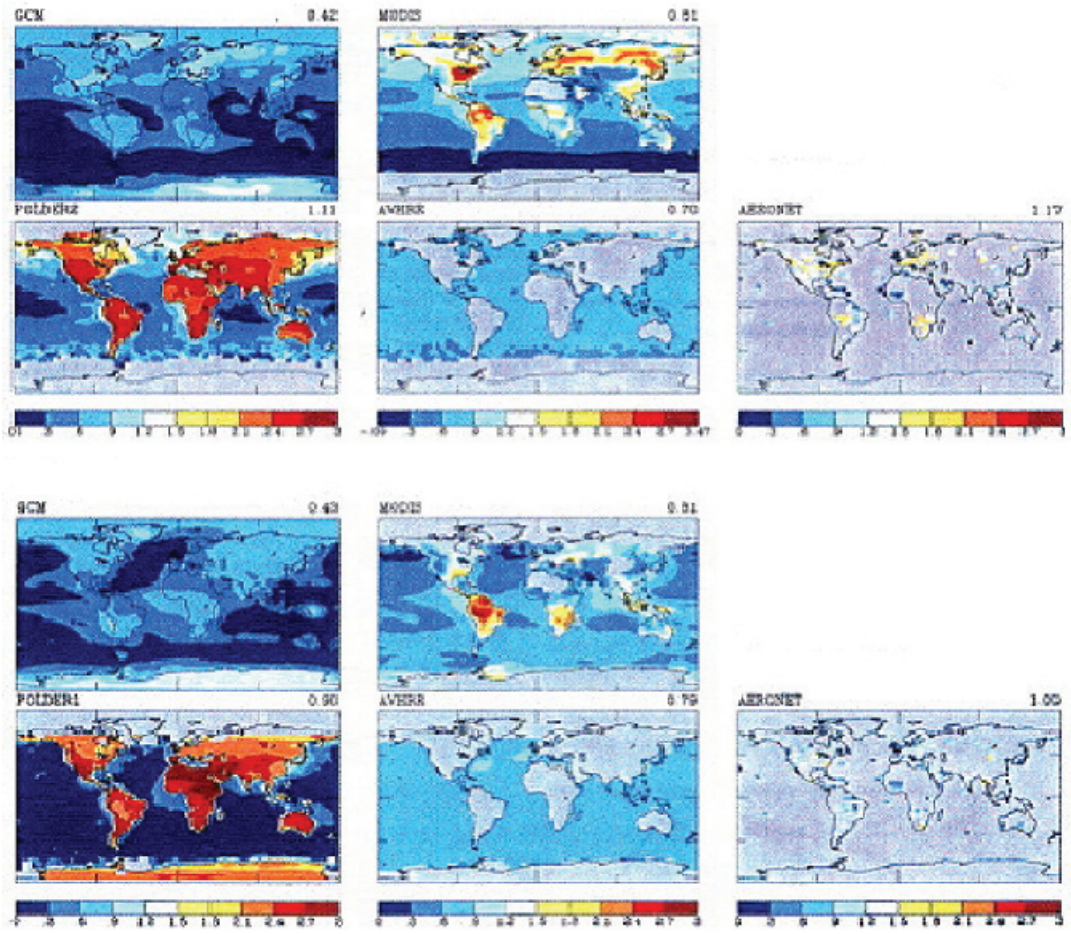


**Fig. 3.8.** GISS GCM Ångstrom exponent compared with observations for June-August (top two rows) and December-February (bottom two rows). Global numbers (area-weighted with missing data skipped) are shown in the right hand corner. From Liu et al. (2006).

As can be seen in the figure, there are large differences among the data sets themselves, and between the observations and the model. Since the Ångstrom exponent is calculated as the logarithmic derivative of aerosol optical depths between two wavelengths, small differences in optical depth as a function of wavelength are magnified; in addition the instruments each use somewhat different wavelengths to make this calculation (e.g., MODIS uses 0.47-0.66 μm over land, and 0.55-0.85 μm over ocean; POLDER uses 0.55-0.865 μm over both land and ocean, AERONET uses 0.47-0.85 μm over land, and AVHRR uses 0.65-0.8 μm). The data sets show higher values over land and lower values over open ocean, due to the increased sea salt component of ocean aerosols (sea salt has a larger particle size). POLDER values are again larger because of the restriction to the accumulation mode (identified at least in part by the Ångstrom value). The GISS model data can be seen to be biased low (e.g., by comparison with MODIS); one explanation would be that the aerosol dry sizes in the GISS GCM climatology are set too large, which would be consistent with the GISS aerosol optical depths being lower than in the satellite observations. The average effective radius in the GISS model appears to be 0.3-0.4 μm, whereas the observational data indicates a value more in the range of 0.2-0.3 μm (Liu et al., 2006).

The model's single scattering albedo (at 0.55 μm) is compared with observations in **Figure 3.9** {adapted from Liu et al. 2006, Fig. 11}. This parameter is important because the higher the value, the less absorption relative to scattering, and the more the aerosols cool the climate, as determined by net radiation at the top of the atmosphere. At the same time, a smaller single scattering albedo reduces the energy available at the surface (as more is absorbed in the atmosphere). Hansen et al. (1997) calculate that the transition from global cooling to heating occurs at a single scattering albedo of ~0.91 with interactive clouds (~0.86 with fixed clouds).

Compared with AERONET data (version 2) {**Figure 3.10**, adapted from Liu et al., 2006, Fig. 12}, the GISS GCM appears to overestimate the single scattering albedo in general (although it underestimates it in Northern Africa and the Persian Gulf), perhaps because black carbon absorption is excessive, or because the particle size is too large.

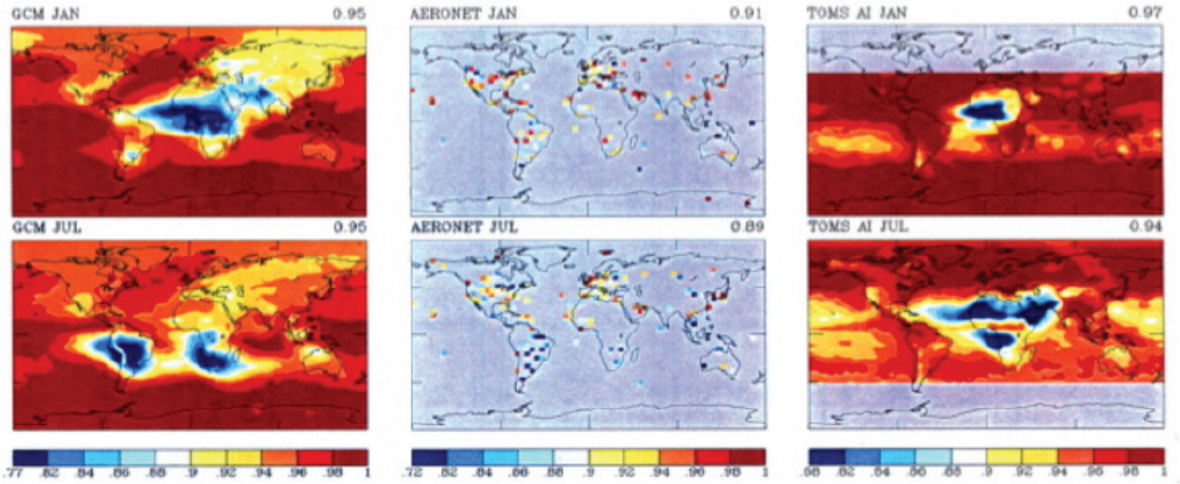


**Fig. 3.9.** January and July monthly mean single scattering albedo compared with AERONET and TOMS data. The TOMS Aerosol Index (AI) (at 0.32 μm for 1990 has been rescaled as ($\varpi$=1-0.1 x AI) to roughly resemble the GCM single scattering albedo. Area-weighted global means are given in the top right-hand corner. From Liu et al. (2006).

To summarize these results: while there are many realistic aspects of the GISS aerosol climatology for the 1990 and later time period, the results suggest that the prescribed sizes are too large, and the optical depth is too small. These are related effects (see equation 1), so both could be improved by reducing the particle size, although as discussed in Chapter 2, errors in aerosol optical depth are primarily due to

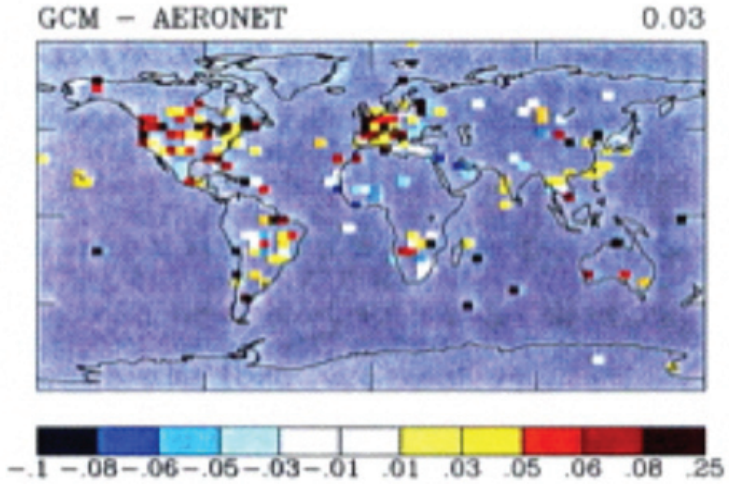


**Fig. 3.10.** GISS GCM minus AERONET single scattering albedo. The value for this GISS model is reported at 0.55 μm while the selected AERONET wavelength is 0.44 μm. From Liu et al. (2006).

sources and transports, not aerosol properties. Underestimation of optical depth leads to underestimation of the aerosol cooling influence. On the other hand, the single scattering albedo appears to be too large, which could be associated with the black carbon emissions used in the aerosol model from which these values are derived. This effect overestimates the aerosol cooling at the top of the atmosphere; it might be ameliorated by redistributing the black carbon aerosol optical depths. Improving all of these features simultaneously while still keeping a reasonable seasonal variation is not a straightforward task, and it is unclear what influence it will have on the net aerosol radiative forcing. Therefore, this comparison does not provide a clear indication of how direct aerosol radiative forcing in the GISS model relates to observations.

To better understand the accuracy of the direct aerosol radiative forcing, Penner et al. (2002) compared model simulations with AVHRR aerosol optical depth and ERBE clear sky reflectance retrievals. The GISS model in use at that time had reduced aerosol optical depths compared with observations at low and southern latitudes, and overall reduced clear-sky shortwave radiative fluxes of several $Wm^{-2}$ at the top of the atmosphere on the global average. As discussed in that study, it is possible that this reduced flux is associated with incomplete cloud screening from the satellite data rather than a model discrepancy; alternatively, there could be a missing non-sea salt open-ocean source that would increase aerosol optical depths in the region 10°N-30°S. One difference between the GISS model used then and the current version used for climate change experiments is that the newer model has an increased single scattering albedo for dust, which would make it somewhat more reflective.

Combining the Penner et al. (2002) and Liu et al. (2006) studies leads to the conclusion that the GISS model may underestimate the organic and sea salt optical thicknesses, and overestimate the influence of black carbon aerosols in the biomass burning regions. To the extent that is true, it would indicate the GISS model underestimates the direct aerosol cooling effect in a substantial portion of the tropics,

If this is due to a missing natural source, errors in the model burden of naturally-produced aerosols such as DMS, sea salt and some organic molecules will not by themselves directly affect cooling relative to preindustrial simulations. They will also not affect future climate change experiments if they are not expected to change significantly, but they could influence the absorption and wet removal of anthropogenic aerosols through internal mixing and scattering.

An additional concern for climate change simulations relates to the aerosol trend in the GISS model. As noted above, the aerosols in the model are kept fixed after 1990. In fact, the observed trend shows a reduction in tropospheric aerosol optical thickness from 1990 through the present, at least over the oceans (Mischenko et al., 2007). Hansen et al. (2007) suggested that the deficient warming in the GISS model over Eurasia post-1990 was due to the lack of this trend. Indeed, a possible conclusion from the Penner et al. (2002) study was that the GISS model overestimated the aerosol optical thickness (presumably associated with anthropogenic aerosols) poleward of 30°N,. However, when an alternate experiment reduced the aerosol optical depths, the polar warming became excessive (Hansen et al., 2007). Another possibility could be that the lack of sufficient warming over Eurasia was the result of the model's insufficiently positive NAO/AO phase for this time period (hence a dynamic issue, independent of aerosols). Again, clarifying this issue requires numerous modeling experiments and various types of observations.

### ***3.2.2.*** *The GFDL Model*

The comparison of observations with the GFDL model reported in the literature is not nearly as extensive as that for the GISS model. Nevertheless, some of the assessments discussed above were performed for this model as well. A comparison between the different models will be given in the next section.

The aerosols used in the GFDL climate experiments are obtained from simulations performed with the MOZART 2 model (Model for Ozone and Related chemical Tracers) (Horowitz et al., 2003) except for dust, which uses sources from Ginoux et al. (2001) and wind fields from NCEP/NCAR reanalysis data. It includes most of the same aerosol species as in the GISS model (although it does not include nitrates), and, as in the GISS model, relates the dry aerosol to wet aerosol optical depth (for sulfate and sea salt but not organic carbon) via the relative humidity. While the parameterizations come from different sources, both models maintain a very large growth in particle size when the relative humidity exceeds 90%. For more details see Ginoux et al. (2006), from which this comparison with observations is based.

Overall, the GFDL global mean aerosol mass loading is within 30% of that of other studies (Chin et al., 2002; Tie et al., 2005; Reddy et al., 2005), except for sea salt which is 2 to 5 times smaller. However, the aerosol optical depth for sulfate ($\tau$ = 0.1) is 2.5 times that of other studies, while the organic carbon value is considerably smaller (on the order of 1/2). Both of these differences are influenced by the relationship with relative humidity, which in the GFDL model for sulfate is allowed to grow up to 100% (but is maintained constant for organic carbon).

Shown in **Figure 3.11** {adapted from Ginoux et al. 2006, Fig. 7} is the comparison of the mean optical depth with AVHRR and MODIS data for the time period 1996-2000. The global mean value over the ocean (0.15) is in good agreement with AVHRR data (0.14 in Fig.3.11) but there are significant

differences regionally, with the model overestimating the value in the northern mid latitude oceans and underestimating it in the southern ocean. Comparison with MODIS also shows good agreement globally (0.15 in Fig. 3.11), but in this case indicates large disagreements over land, with the model producing excessive aerosol optical depth over industrialized countries and underestimating the effect over biomass burning regions.

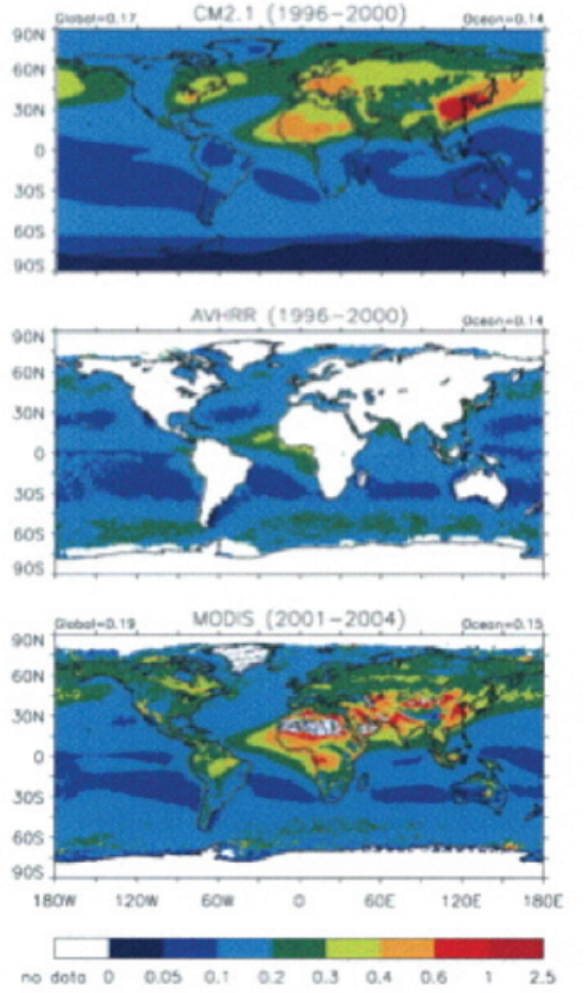


**Fig. 3.11.** Comparison of mean optical depth at 0.55 μm in the GFDL model C2.1 (1996-2000 average) (top) with AVHRR (1996-2000 average) (middle) and MODIS (2001-2004 average) (bottom). From Ginoux et al. (2006).

Comparison with AERONET data is given in **Figure 3.12** {adapted from Ginoux et al., 2006, Fig. 8}. The correlation between simulated and observed values is 0.6. In agreement with the satellite comparison, the model overestimates the aerosol optical depth in polluted regions of the Northern Hemisphere by a factor of 2 and underestimates the optical depth in biomass burning regions by a factor of 2.

Comparisons of the model's results have also been performed with other data sets (e.g., from the University of Miam; from the IMPROVE program at sites located in U.S. National Parks; and from the EMEP program at stations spread about 27 countries in Europe; for appropriate references, see Genoux et al., 2006). The results show that sulfate optical depth is overestimated in spring and summer (and underestimated in winter) in many regions, including Europe and North America, due perhaps to the relative humidity relationship at high humidities, or perhaps to insufficient removal mechanisms. Organic and black carbon aerosols are also overestimated in polluted regions by a factor of two, where-

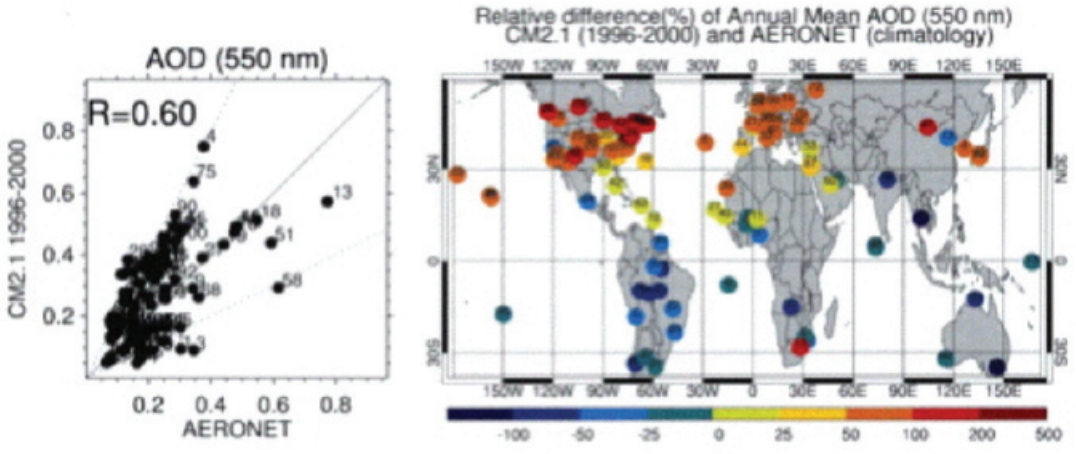


**Fig. 3.12.** Comparison of GFDL GCM aerosol optical depth at 0.55 μm with aerosol observations (left) and relative differences at each location (right). From Ginoux et al. (2006).

as organic carbon aerosols are elsewhere underestimated by factors of 2 to 3. Dust concentrations at the surface agree with observations to within a factor of 2 in most places where significant dust exists, although over the southwest U.S. it is a factor of 10 too large. Sea salt surface concentrations are underestimated by more than a factor of 2. Over the oceans, the excessive sulfate optical depths compensate for the low sea salt values; this is not true over the southern ocean where, in the real world, high wind speeds result in large amounts of sea salt, so here the model's total optical depth is underestimated by a factor of 2.

Therefore, from an optical depth standpoint, the good global-average agreement masks an excessive aerosol loading over the Northern Hemisphere (in particular, over the northeast U.S. and Europe) and an underestimate over biomass burning regions and the southern oceans. No specific comparison was given for particle size or single-scattering albedo, but the excessive sulfate would likely produce too high a value of reflectivity relative to absorption except in some polluted regions where black carbon (an absorbing aerosol) is also overestimated.

### ***3.2.3.*** *Model Intercomparisons*

The above discussion, along with Tables 3.1 and 3.2, allows for some synthesis as to the realism of these models' aerosol distribution and how the models rank with respect to other models. With respect to observations, first for sulfates, the GISS model has values less than or equal to the observed for optical depth and radiative impact, while the GFDL model overestimates it by a factor of two. The comparison shown in Table 3.1 indicates that the GISS model direct effect for sulfate is among the highest of the models reviewed; this would imply that the GFDL model values are too large within the context of other models.

For black carbon with respect to observations, the GISS model appears to overestimate its influence in the biomass burning regions and underestimate it elsewhere, while the GFDL model is somewhat the reverse: it overestimates it in polluted regions, and underestimates it in biomass burning areas. The global comparison shown in Table 3.2 indicates the GISS model has values similar to those from other

models, which might be the result of such compensating errors. The GISS and GFDL models have relatively similar global-average black carbon contributions, and the same appears true for organic carbon.

The GISS model has a much larger sea-salt contribution than does GFDL (or indeed other models), a result that is dominated by the southern hemisphere distribution.

As for regional variations, an approximate comparison of the GISS and GFDL model optical depths can be obtained by comparing **Fig. 3.11** with **Figs. 3.4**. Overall there is reasonable agreement in magnitude, with some regional differences, e.g., polluted regions at mid-latitudes have greater optical depth in the GFDL model, while GISS values are larger in low latitude biomass burning regions. The contributions to this clear-sky direct effect from the different aerosol components shows a greater disparity (**Fig. 3.13 a,b**), as can be seen for example over the Southern Ocean, where the primary influence is sea salt in the GISS model {Fig. 3.13 (left), from Lacis, 2007, personal communication}, while in the GFDL model it is sulfate {Fig. 3.13 (right) adapted from Ginoux et al., 2006}. Ginoux et al. (2006) suggest that the sulfate result is due to excessive relative humidity contribution at the highest humidities, although the GISS model uses a formulation that also produces large increases at the highest humidities and its results are very different. The particularities in the parameterization of sulfate removal from the atmosphere may be involved. Since the GISS global optical depth is 0.15 and the GFDL value is 0.17, these regional proportional differences can also be used to indicate component optical depth differences.

No extensive published comparison with observations is available from the NCAR model, but CCSP 3.2 reviewed some characteristics of the aerosol loading from that model with respect to the GFDL and GISS

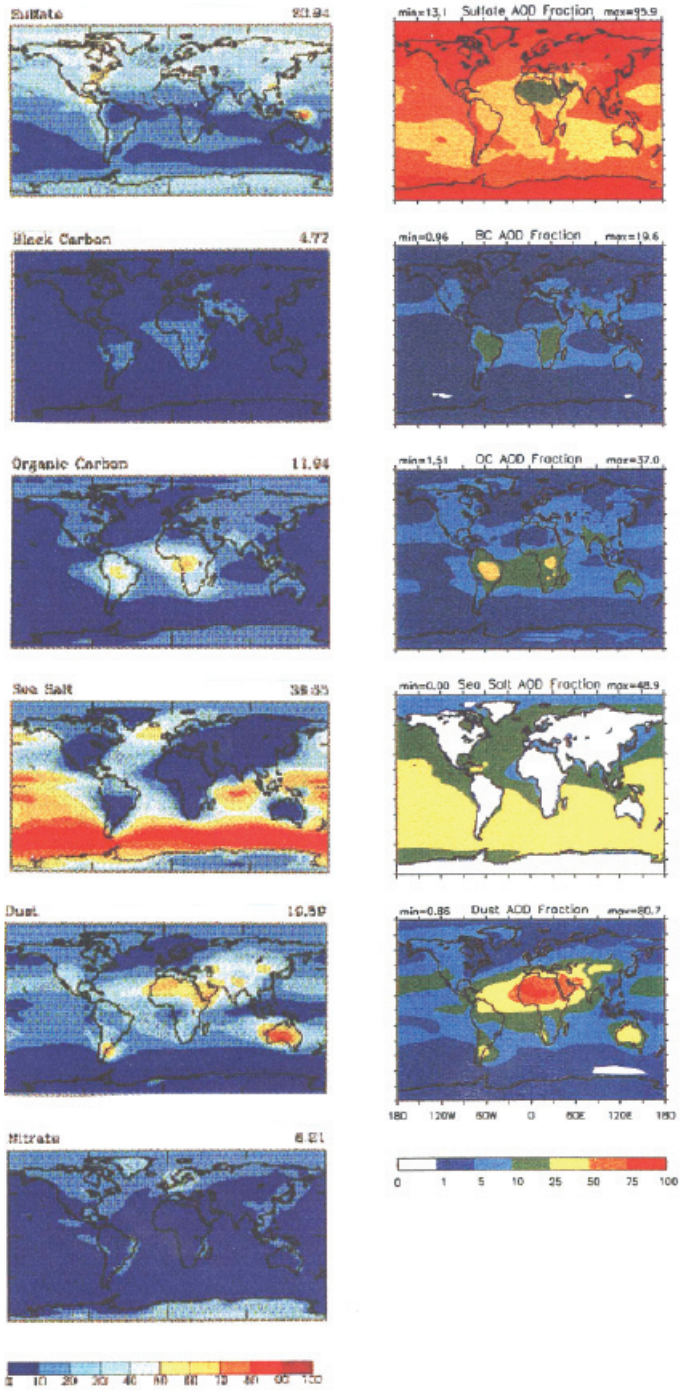


**Fig. 3.13.** Percentage of aerosol optical depth in the GISS (left) and GFDL (right) models associated with the different components. GFDL does not have nitrate aerosols. Note the different color bars. From Liu et al. (2006) and Ginoux et al. (2006).

values. Sulfates provide the greatest contribution to total aerosol optical depth in the NCAR model for present day donations; its sulfate optical depth is greater than in the GISS model but less than for GFDL (where it dominates the total). The NCAR sea salt value is considerably smaller than that for GISS (where it dominates the total). Hence the NCAR total aerosol optical depth is only about 2/3 the GISS and GFDL values, and appears to be too small compared with satellite retrievals.

The global average direct aerosol radiative forcing at the top of the atmosphere as calculated by various models, including several variants of the GISS model, and as inferred from observations, is presented in **Figure 3.14** {adapted from IPCC 2007 Fig. 2.13}. Note the wide range of forcing. Even amongst the various GISS model simulations the magnitude differs substantially. Part of this result is due to changing aerosol sources or sulfate production in clouds in the different GISS studies, but a major influence is the question of whether aerosol particles are internally or externally mixed (see Section 3.2d). The comparison with observations suggests that most models underestimate the direct effect on a global scale, although the differences only amount to a few tenths $Wm^{-2}$ (and the observations themselves have significant uncertainties – see Chapter 2).

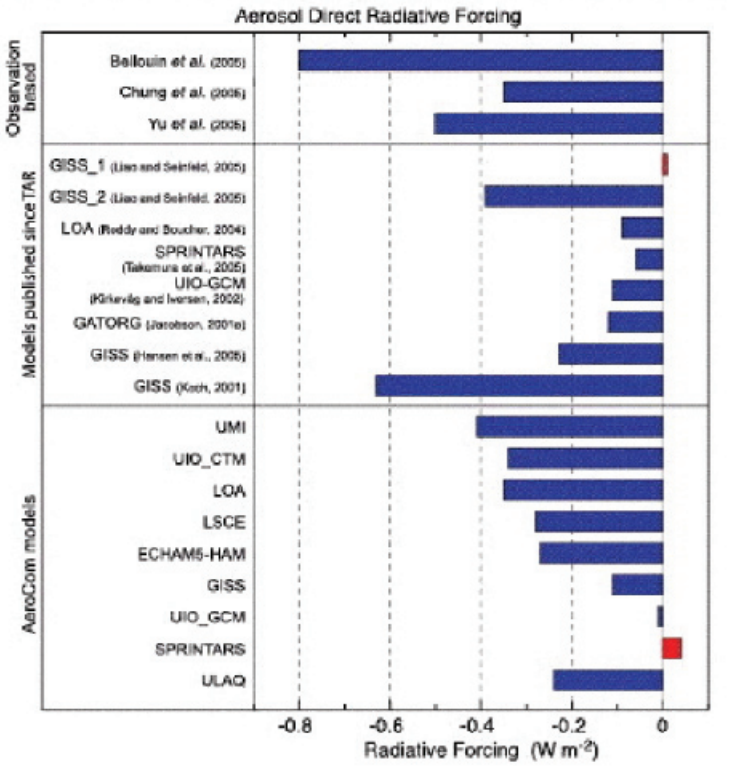


**Figure 3.14.** Aerosol direct radiative forcing in various climate and aerosol models. Observed values are shown in the top section. From IPCC (2007).

A further comparison can be made with the chemical transport models that participated in the Aerocom intercomparison (see also Table 3.2) (Schulz et al., 2006). Aerosol and radiative results from these models are shown in **Figure 3.15** {adapted from IPCC 2007 Fig. 2.12}. The total aerosol optical depth is somewhat lower in these models than in the observations, similar to the GISS model results (however MODIS tends to overestimate aerosol optical depth over land, where MISR is more realistic). With respect to the radiative forcing due to anthropogenic aerosols, at the top of the atmosphere,

the Aerocom models had negative forcings of -0.5-2 $Wm^{-2}$ in biomass burning and polluted regions, with small, positive forcing elsewhere (Fig. 3.15, lower left). The GISS model {Figure 3.16, upper left, adapted from Lacis 2007 personal communication} has occasional larger negative values in polluted regions, and somewhat stronger positive forcing at the highest latitudes. The differences are even larger at the surface, with the GISS model exceeding –4 $Wm^{-2}$ over large regions (Fig. 3.16, lower left), an

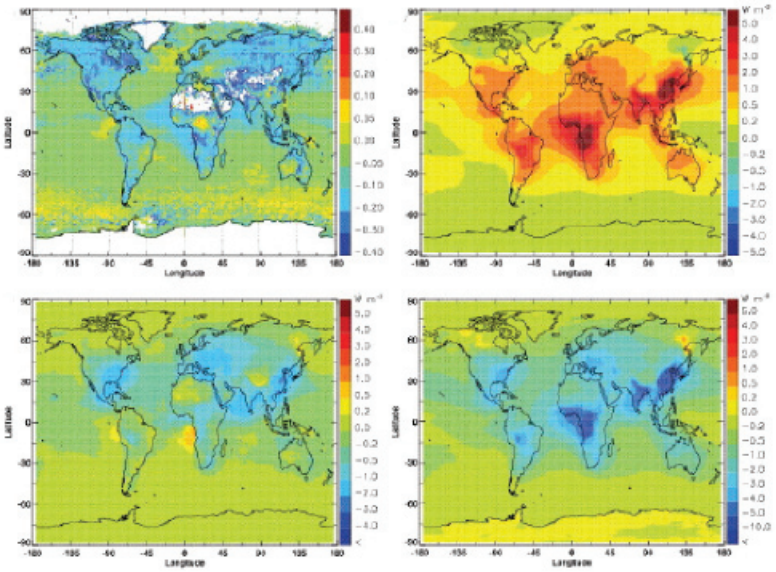

**Fig. 3.15.** Average results from the nine AeroCom models listed in Table 3.2. Upper left: difference in aerosol optical depth between the models and MODIS data [note the expanded scale compared with that in the lower right]; lower left, upper right and lower right: anthropogenic aerosol shortwave radiative forcing at the top of the atmosphere, of the atmosphere, and at the surface, respectively.

effect only seen in particular regions in the average of the Aerocom models (Fig. 3.15, lower right). This would seem to be due to larger optical depths in the GISS climate model in these regions, specifically the enhancement of black and organic carbon assumed for the climate change simulations (as indicated in the introduction, this was to better match AERONET data. The GISS model version contributed to AEROCOM lacked such enhancement.). The bias in the other GISS aerosol parameters, such as the single-scattering albedo (too high) and particle size (too large) would actually give smaller surface forcing.

A prerequisite to accurately representing aerosols in chemical transport models and climate models is understanding the chemical reactions responsible for aerosol formation. Numerous issues remain uncertain, and the full scope of the problem is outside the framework of this document. A discussion of one important issue relating to secondary organic aerosol formation is included as Appendix A.2.

Some of the conclusions derived from the comparison of the GISS and GFDL climate models illustrate results that are applicable to models in general, including aerosol models. From an assessment of more than 20 aerosol model simulations used for Aerocom intercomparison, Kinne et al. (2006) concluded that aerosol models being run in 2005 do a better job of matching total optical thicknesses from observations than was true in 2002, but there are large differences among aerosol types in how it is done (a conclusion also reached by Schulz et al., 2006). This will affect the direct anthropogenic radiative forcing, which depends on the components (particularly for sulfates, organic and black carbon aerosols). Model mean aerosol concentrations look to be too large over land (outside of the tropics), and too small over oceans and tropical land. Model aerosol sizes are too large over the Northern Hemi-

sphere, and too small over biomass burning regions. The vertical distribution of aerosols differs among models. There are also large model differences in dust, carbonaceous aerosols, the aerosol water mass, and the absorption potential (because of large differences in aerosol composition); in general, models have too little aerosol absorption. Bates et al. (2006) found that in polluted regions the chief causes of the inter-model differences for the clear sky, direct forcing are the differences in emissions, followed by differences in wet removal. However, even when emissions are harmonized, removal processes and transport differences produce large variations among the models (Textor et al., 2007).

### ***3.2.4.*** *Additional considerations*

Also shown in **Fig. 3.16** (right column) is the aerosol long wave forcing, which will also be affected by the particular aerosol characteristics used in each model. However, compared to the short wave forcing, the values are on the order of 10%, and therefore insignificant considering the other uncertainties. Of more importance is the vertical distribution of the aerosols. This aspect is of secondary importance

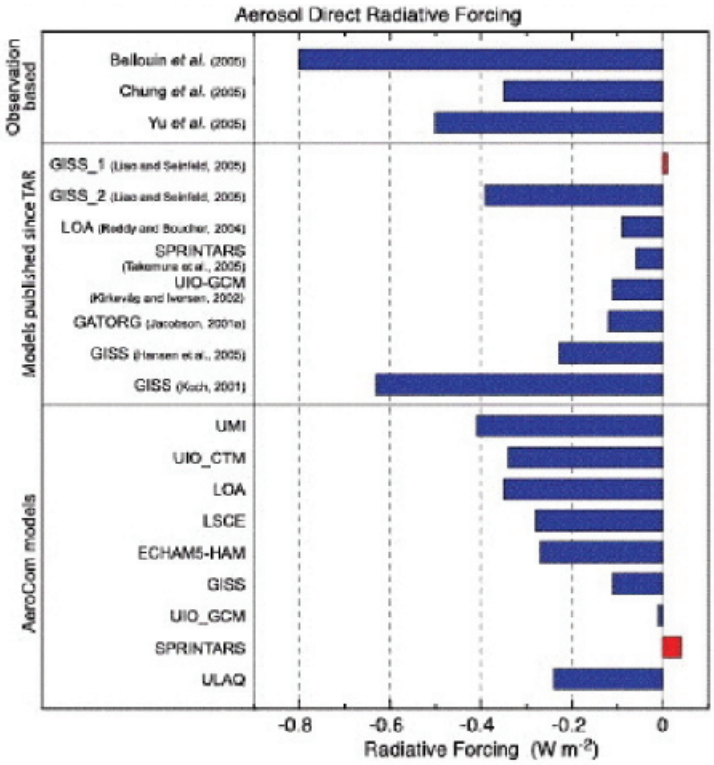


**Fig. 3.16.** Direct radiative forcing by anthropogenic aerosols in the GISS model (including sulfates, BC, OC and nitrates). Short wave forcing at the top and bottom of the atmosphere are shown in the top left and bottom left panels. The corresponding thermal forcing (discussed later) is indicated in the right hand panels. From Lacis et al. (2007) (personal communication).

for non-absorbing aerosols (except when considering humidification effects and the vertical distribution of water vapor), but absorbing aerosols will reradiate energy depending on their temperature (and hence altitude). Presented in **Fig. 3.17** {adapted from Lacis 2007 personal communication} is the mean pressure level for aerosols in the GISS model for January and July. Sulfate and sea salt lead to the average aerosol being located in the lowest 3 km, but the altitudes to which biomass burning aerosols are lofted has a large impact on their net radiative forcing. This feature needs to be compared with observations and among the models.

Most climate model simulations incorporating different aerosol types have been made using external mixtures, i.e., the evaluation of the aerosols and their radiative properties are calculated separately for each aerosol types. Observations indicate that aerosols commonly consist of internally mixed particles, and these 'internal mixtures' can have very different radiative impacts; compare, for example, the GISS-1 (internal mixture) and GISS-2 (external mixture) model results shown in **Figure 3.14**, a difference between slight warming and significant cooling (due to both changes in radiative properties of the mixtures, and changes in aerosol amount). The more sophisticated aerosol mixtures now being initiated in different modeling groups may well end up producing very different direct (and indirect) forcing values.

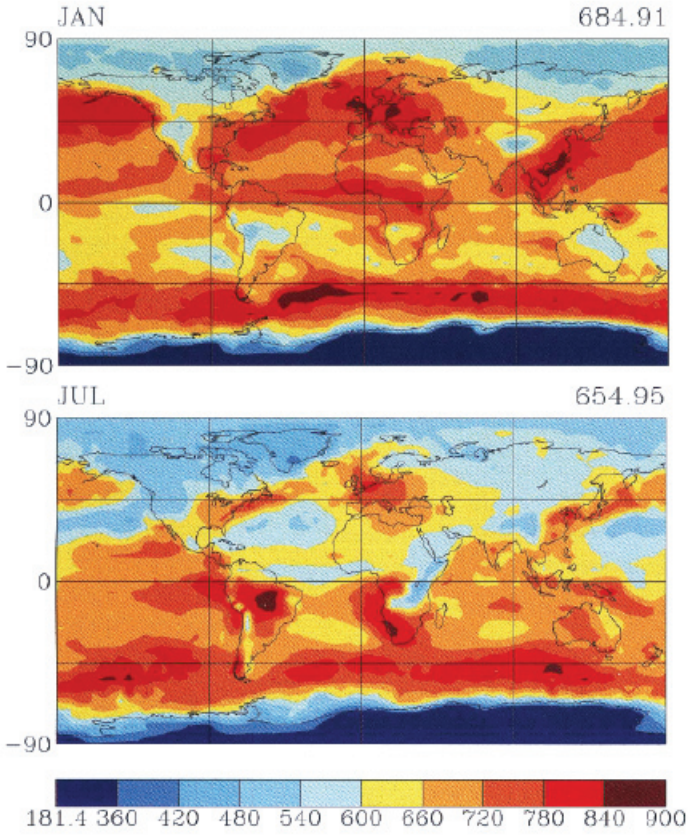


**Fig. 3.17.** Mean pressure level of the GISS GCM aerosol for January and July (Lacis, 2007, personal communication).

Finally, comparisons with satellite data are concerned with clear-sky aerosol optical thickness and radiative effect. As shown in **Fig. 3.18** {adapted from Lacis, 2007, personal communication}, the aerosol optical depth is larger in cloudy-sky conditions because of the hygroscopic nature of sulfate, which is modeled as a function of relative humidity. Aerosols above or below clouds do not have any significant direct scattering effects, since the cloud reflectivity is much larger. (Absorbing aerosols above clouds would have a strong positive forcing.) However, recent work (Wen et al., 2007) indicates that the enhanced reflections of light between clouds can even have a strong impact on the direct radiative effect of aerosol residing in cloud-free regions. These aspects illustrate the complexity of the system and the difficulty of representing aerosol radiative influences in GCMs, whose cloud distribution is somewhat problematic. And of course aerosols in cloudy regions can affect the clouds themselves, as are discussed in the next section.

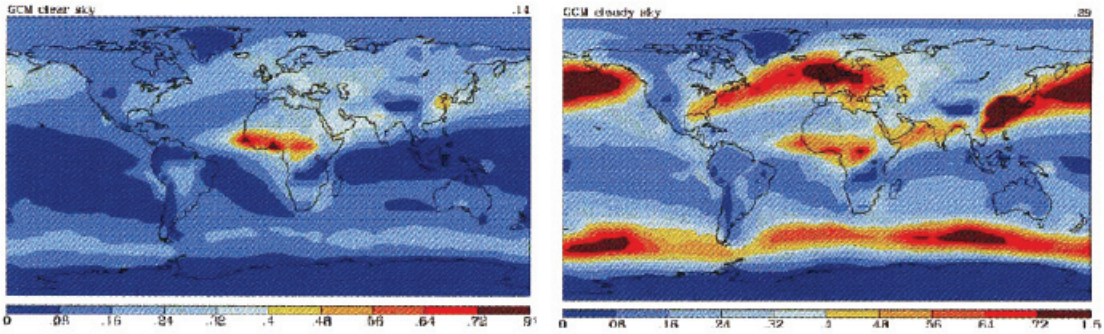

**Fig. 3.18.** GISS aerosol optical depth for clear skies (left) and cloudy-sky conditions (right). Global mean values at 0.55 μm are shown in upper right hand corners. From Lacis 2007, personal communication.

## 3.3. Comparison of the Aerosol Indirect Effect in GCMs

### *3.3.1. Aerosol effects on clouds and radiation*

A subset of the aerosol particles can act as cloud condensation nuclei (CCN) and/or ice nuclei (IN). Increases in aerosol particle concentrations, therefore, may increase the ambient concentrations of CCN and IN, affecting cloud properties. For a fixed cloud liquid water content, a CCN increase will lead to more cloud droplets, and so the cloud droplet size will decrease. That effect leads to brighter clouds, the enhanced albedo then being referred to as the 'cloud albedo effect' (Twomey, 1977). If the droplet size is smaller, it may take longer to rainout, leading to an increase in cloud lifetime, hence the 'cloud lifetime' effect (Albrecht, 1989). As noted in Table 3.3, approximately one-third of the models used for the IPCC 20th century climate change simulations incorporated an aerosol indirect effect, generally (though not exclusively) associated with sulfates.

The representation of these first and second indirect effects as relatively simple constructs in GCMS will be considered below. However, it is becoming increasingly clear from studies based on high resolution simulations of aerosol-cloud interactions that there is a great deal of complexity that is unresolved in GCMs. We return to this point in section 3.3.3.

The net radiative forcing produced in various model studies associated with the cloud albedo effect was shown in **Figure 3.3**. It ranges from –0.25 to –1.8 $Wm^{-2}$. The IPCC estimate given in the introduction ranges from +0.4 to –1.1 $Wm^{-2}$, with a 'best-guess' estimate of –0.7 $Wm^{-2}$.

Most models did not incorporate the 'cloud lifetime effect'. Hansen et al. (2005) compared this latter influence (in the form of time-averaged "cloud area" or cloud cover increase) with the cloud albedo effect. In contrast to the discussion in IPCC (2007), they argue that the cloud cover effect is more likely to be the dominant one, as suggested both by cloud-resolving model studies (Ackerman et al., 2004) and satellite observations (Kaufman et al., 2005). The cloud albedo effect may be partly offset by reduced cloud thickness accompanying aerosol pollutants, hence a meteorological (cloud) rather than aerosol effect (see the discussion in Lohmann and Feichter, 2005). (The distinction between meteorological feedback and aerosol forcing can become quite opaque.) Nevertheless, both aerosol

indirect effects were utilized in the GISS model, related to an increase in aerosol cloud droplet number concentration, a function of sulfate, nitrate, black carbon and organic carbon concentration. Only the low altitude cloud influence was modeled, principally because there are greater aerosol concentrations at low levels, and because low clouds currently have greater cloud radiative forcing. [The influence on high altitude clouds, associated with IN changes, is a relatively unexplored area for GCMs and as well for process-level understanding.]

A comparison of the GISS direct and two indirect effects is shown in **Figure 3.19** {adapted from Hansen et al., 2005, Figure 13}. As parameterized, the second indirect effect produced somewhat greater negative radiative forcing and cooling, but this was the result of constants tuned to give that response. Geographically, it appears that the 'cloud cover' effect produced slightly more cooling in the Southern Hemisphere than did the 'cloud albedo' response, with the reverse being true in the Northern Hemisphere.

There are many different aspects that can explain the large divergence of indirect effects in models (Fig. 3.3). To explore this in more depth, Penner et al. (2006) used three different GCMs to analyze the differences between models for the first indirect effect, as well as a combined first plus second indirect effect. The models all had different cloud and/or convection schemes.

In the first experiment, the monthly average aerosol mass and size distribution of, effectively, sulfate aerosol were prescribed, and all models followed the same prescription for parameterizing the cloud droplet number concentration as a function of aerosol concentration. In that sense, the only difference

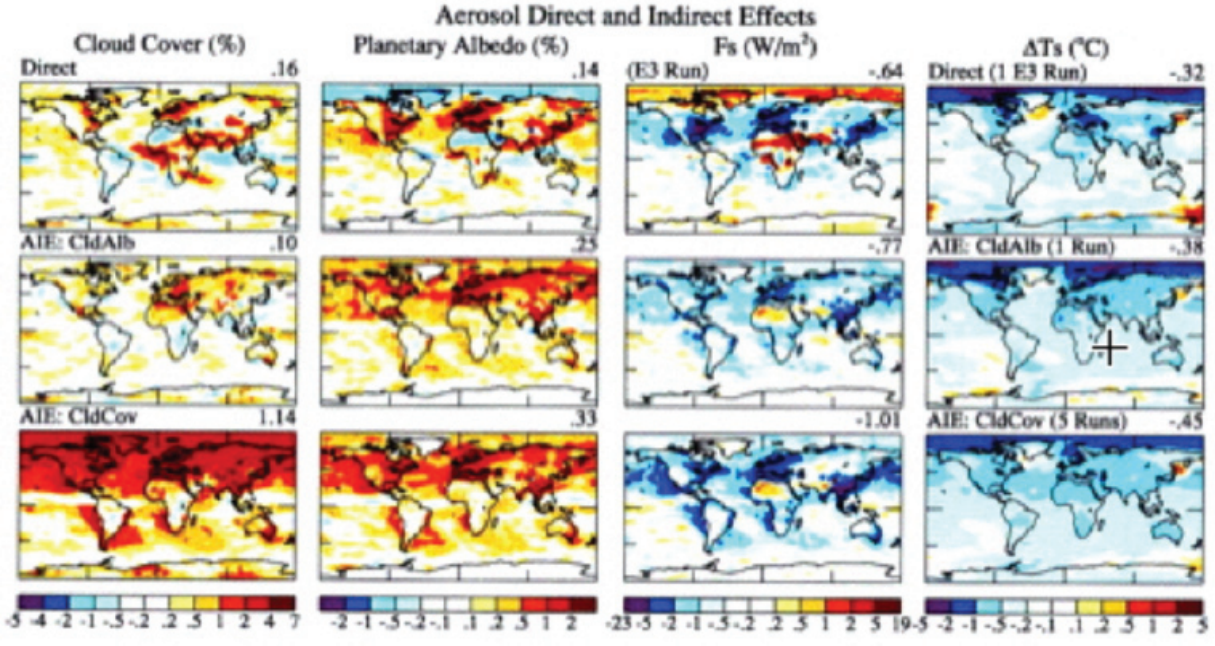


**Fig. 3.19.** Anthropogenic impact on cloud cover, planetary albedo, radiative flux at the surface (while holding sea surface temperatures and sea ice fixed) and surface air temperature change from the direct aerosol forcing (top row), the 1st indirect effect (second row) and the second indirect effect (third row). The temperature change is calculated from years 81-120 of a coupled atmosphere simulation with the GISS model. From Hansen et al., (2005).

among the models was their separate cloud formation and radiation schemes. The different models all produced a similar droplet effective radii, and therefore shortwave cloud forcing, and change in net outgoing whole sky radiation between pre-industrial times and the present. Hence the first indirect effect was not a strong function of the cloud or radiation scheme. The results for this and the following experiments are presented in **Figure 3.20**, where the experimental results are shown sequentially from left to right {adapted from Penner et al., 2006 Fig. 5} for the whole sky effect, and in Table 3.4 {adapted from Penner et al., 2006, Table 3} for the clear-sky and cloud forcing response as well.

In the second experiment, the aerosol mass and size distribution were again prescribed, but now each model used its own formulation for relating aerosols to droplets. In this case one of the models produced larger effective radii and therefore a much smaller first indirect aerosol effect (Figure 3.20, Table 3.4). However, even in the two models where the effective radius change and net global forcing were similar, the spatial patterns of cloud forcing differ, especially over the biomass burning regions of Africa and South America.

The third experiment allowed the models to relate the change in droplet size to change in precipitation efficiency (i.e., they were now also allowing the second indirect effect - smaller droplets being less efficient rain producers – as well as the first). The models utilized the same relationship for autoconversion of cloud droplets to precipitation. All models produced an increase in cloud liquid water path, and all produced a smaller effect on cloud fraction in (absolute value) than in the previous experiments with the first indirect effect. For two of the models the net impact on outgoing shortwave radiation was to increase the negative forcing by about 20%, while in the third model (which had the much smaller first indirect effect) the radiative forcing was magnified by a factor of three.

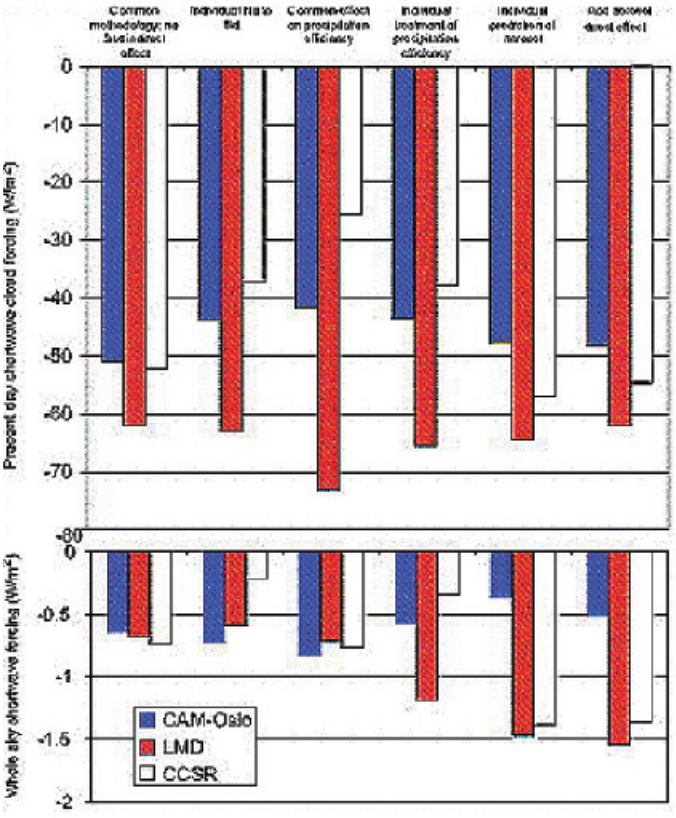


**Fig. 3.20.** Global average present day short wave cloud forcing at the top of the atmosphere (top) and change in whole sky net outgoing shortwave radiation (bottom) between the present-day and pre-industrial simulations for each model in each experiment. From Penner et al. 2006.

**Table 3.4.** Differences in present day and pre-industrial outgoing solar radiation in the different experiments. From Penner et al. (2006).

| | exp. 1 | exp. 2 | exp. 3 | exp. 4 | exp. 5 | exp. 6 |
|---|---|---|---|---|---|---|
| Whole-sky | | | | | | |
| CAM-Oslo | -0.648 | -0.726 | -0.833 | -0.580 | -0.365 | -0.518 |
| LMD-Z | -0.682 | -0.597 | -0.722 | -1.194 | -1.479 | -1.553 |
| CCSR | -0.739 | -0.218 | -0.773 | -0.350 | -1.386 | -1.386 |
| Clear-sky | | | | | | |
| CAM-Oslo | -0.063 | -0.066 | -0.026 | 0.014 | -0.054 | -0.575 |
| LMD-Z | -0.054 | 0.019 | -0.066 | -0.066 | -0.126 | -1.034 |
| CCSR | 0.018 | -0.0068 | -0.045 | -0.008 | 0.018 | -1.168 |
| CAM-Oslo | -0.548 | -0.660 | -0.807 | -0.595 | -0.311 | 0.056 |
| LMD-Z | -0.628 | -0.616 | -0.752 | -1.128 | -1.353 | -0.518 |
| CCSR | -0.757 | -0.212 | -0.728 | -0.342 | -1.404 | -0.200 |

In the fourth experiment, the models were now each allowed to use their own formulation to relate aerosols to precipitation efficiency. This introduced some additional changes in the whole sky shortwave forcing (Fig. 3.20).

In the fifth experiment, models were allowed to produce their own aerosol concentrations, but were given common sources. This produced the largest changes in the radiative forcing in several of the models. Within any one model, therefore, the change in aerosol concentration has the largest effect on droplet concentrations and effective radii. This experiment too resulted in large changes in radiative forcing.

In the last experiment, the aerosol direct effect was included, based on the full range of aerosols used in each model. While the impact on the whole-sky forcing was not large, the addition of aerosol scattering and absorption primarily affected the change in clear sky radiation (**Table 3.4**).

The results of this study emphasize that in addition to questions concerning cloud physics, the differences in aerosol concentrations among the models (i.e., Figs. 3.4, 3.11 and 3.15) play a strong role in inducing differences in the indirect effect(s), as well as the direct one.

Observational constraints on climate model simulations of the indirect effect with satellite data (e.g. MODIS) have been performed previously in a number of studies (e.g. Storelvmo et al. 2006, Lohmann et al. 2006, Quaas et al. 2006, Menon et al. 2007). These have been somewhat limited since satellite retrieved data do not have the vertical profiles needed to resolve aerosol and cloud fields (e.g. cloud droplet number and liquid water content), and the temporal resolution of simultaneous retrievals of aerosol and cloud products are usually not available at a frequency of more than one a day. Thus, the indirect effect, especially the second indirect effect, remains, to a large extent, unconstrained by satellite observations. However, improved measurements of aerosol vertical distribution from the newer generation of sensors on the A-train platform may provide a better understanding of changes to cloud properties from aerosols.

### ***3.3.2.*** *Additional aerosol influences*

Various observations have empirically related aerosols injected from biomass burning or industrial processes to reductions in rainfall (e.g., Warner, 1968; Eagan et al., 1974; Andreae et al., 2004; Rosenfeld, 2000). There are several potential mechanisms associated with this response.

In addition to the two indirect aerosol effects noted above, a process denoted as the 'semi-direct" effect involves the absorption of solar radiation by aerosols such as black carbon, within or in the vicinity of clouds. The absorption increases the temperature, lowering the relative humidity, producing evaporation and hence a reduction in cloud liquid water. The impact of this process depends strongly on what the effective aerosol absorption actually is; the more absorbing the aerosol, the larger the potential positive forcing on climate (by reducing low level clouds and allowing more solar radiation to hit the surface). This effect is responsible for shifting the critical value of $\varpi$ (separating aerosol cooling from aerosol warming) from 0.86 with fixed clouds to 0.91 with varying clouds (Hansen et al., 1997). Reduction in cloud cover and liquid water is one way aerosols could reduce rainfall.

More generally, aerosols can alter the location of solar radiation absorption within the system, and this aspect alone can alter climate and precipitation even without producing any change in net radiation at the top of the atmosphere (the usual metric for climate impact). By decreasing solar absorption at the surface, aerosols (from both the direct and indirect effects) reduce the energy available for evapotranspiration, potentially resulting in a decrease in precipitation. This effect has been suggested as the reason for the decrease in pan evaporation over the last 50 years (Roderick and Farquhar, 2002). This decline in solar radiation at the surface appears to have ended in the 1990s (Wild et al., 2005), perhaps because of reduced aerosol emissions in industrial areas (Kruger and Grasl, 2002).

Energy absorption by aerosols above the boundary layer can also inhibit precipitation by warming the air at altitude relative to the surface, i.e., increasing atmospheric stability. The increased stability can then inhibit convection, affecting both rainfall and atmospheric circulation (Ramanathan et al., 2001; Chung and Zhang, 2004). To the extent that aerosols decrease droplet size and reduce precipitation efficiency, this effect by itself could result in lowered rainfall values locally. In their latest simulations, Hansen et al. (2007) did find that the indirect aerosol effect reduced tropical precipitation; however, the effect is similar regardless of which of the two indirect effects is used, and also similar to the direct effect, so it is likely the result of aerosol induced cooling at the surface and consequent reduced evapotranspiration more than anything else. Similar conclusions were reached by Yu et al. (2002) and Feingold et al. (2005).

The local precipitation change, through its impacts on dynamics and soil moisture, can have large positive feedbacks. Harvey (2004) concluded from assessing the response to aerosols in 8 coupled models that the aerosol impact on precipitation was larger than on temperature. He also found that the precipitation impact differed substantially among the models, with little correlation among them.

### ***3.3.3.*** *Results based on high resolution modeling of aerosol-cloud interactions*

By necessity, the representation of the interaction between aerosol and clouds in GCMs is poorly resolved. This stems in large part from the fact that GCMs do not resolve convection on their large grids

(order several hundred km), that their treatment of cloud microphysics is rather crude, and that as discussed previously, their representation of aerosol needs improvement. Superparametrization efforts (where standard cloud parameterizations in the GCM are replaced by resolving clouds in each grid column of the GCM via a cloud resolving model, e.g., Grabowski, 2004) could lead the way for the development of more realistic cloud fields and thus improved treatments of aerosol-cloud interactions in large-scale models. However these are just being incorporated in models that resolve both cloud and aerosols. Detailed cloud parcel models have been developed to focus on the droplet activation problem (under what conditions droplets actually start forming) and questions associated with the first indirect effect. The coupling of aerosol and cloud modules to dynamical models that resolve the large turbulent eddies associated with vertical motion and clouds (henceforth, large eddy simulations or LES, with grid sizes of ~ 100 m and domains ~ 10 km) has proven to be a powerful tool for representing the details of aerosol-cloud interactions together with feedbacks (e.g., Feingold et al. 1994; Kogan et al. 1994; Stevens et al, 1996; Feingold et al. 1999; Ackerman et al. 2004). In this section we explore some of the complexity in the aerosol indirect effects revealed by such studies to illustrate how difficult parameterizing these effects properly in GCMs could really be.

a. The first indirect effect

The relationship between aerosol and drop concentrations (or drop sizes) is a key piece of the first indirect effect puzzle. It should not however, be equated to the first indirect effect which concerns itself with the resultant radiative forcing. A huge body of measurement and modeling work points to the fact that drop concentrations do indeed increase with increasing aerosol. The main unresolved questions relate to the degree of this effect, and the relative importance of aerosol size distribution, composition and updraft velocity in determining drop concentrations (for a review, see McFiggans et al., 2006). Studies indicate that the aerosol number concentration and size distribution are the most important factors. Updraft velocity (unresolved by GCMs) is particularly important under polluted conditions.

Although there are likely some composition effects that may have significant effect on drop number concentrations, composition is regarded as relatively unimportant compared to the other parameters (Fitzgerald, 1975; Feingold, 2003; Ervens et al., 2005; Dusek et al., 2006). Nevertheless, there are times when composition has a noticeable effect (see Appendix A.3). It has been stated that the significant complexity in aerosol composition can be modeled, for the most part, using fairly simple parameterizations that reflect the soluble and insoluble fractions (e.g., Rissler et al. 2004), yet composition cannot be ignored (an example is shown in Appendix A.3). Furthermore, chemical interactions cannot be overlooked. A large uncertainty remains concerning the impact of organic species on cloud droplet growth kinetics, and thus cloud droplet formation. Cloud drop size is affected by wet scavenging, which depends on composition. And future changes in composition will presumably arise due to biofuels/biomass burning and a reduction in sulfate emissions, which emphasizes the need to include composition changes in climate models when assessing the first indirect effect. The "sulfate plus insoluble" paradigm may become less applicable than is currently the case.

The updraft velocity, and its change as climate warms, may be the Achilles heel of GCMs because it is a key part of convection and the spatial distribution of condensate, as well as droplet activation. Numerous solutions to this problem have been sought, including estimation of vertical velocity based on predicted turbulent kinetic energy from boundary layer models (Lohmann et al., 1999; Larson et al.,

2001) and PDF representations of subgrid quantities, such as vertical velocity and the vertically-integrated cloud liquid water ('liquid water path', or LWP) (Pincus and Klein, 2000; Golaz et al., 2002a,b; Larson et al., 2005). Embedding cloud resolving models within GCMs is also being actively pursued (Grabowski et al. 1999; Randall et al., 2003). Numerous other details come into play; for example, the treatment of cloud droplet activation in GCM frameworks is often based on the assumption of adiabatic conditions, which may overestimate the sensitivity of cloud to changes in CCN (Sotiropoulou et al., 2006, 2007). It will take extensive observations, under difficult conditions, to clarify the requisite cloud and aerosol physics.

b. Other indirect effects

The second indirect effect is often referred to as the "cloud lifetime effect", based on the premise that clouds that do not precipitate will live longer. In GCMs the "lifetime effect" is equivalent to changing the representation of precipitation production and can be parameterized as an increase in cloud area or cloud cover (e.g., Hansen et al., 2005). The second indirect effect hypothesis relates increased aerosol to increased drop concentrations, smaller drops, suppressed collision-induced rain, and longer cloud lifetime. It is curious that, other than the suppression of rain in warm clouds (Warner 1968), there is no clear observational support for this chain of events. Results from ship-track studies show that cloud water may increase or decrease in the tracks (Coakley and Walsh, 2002) and satellite studies suggest similar results for warm boundary layer clouds (Han et al. 2002). Ackerman et al. (2004) used LES to show that in stratocumulus, cloud water may increase or decrease in response to increasing aerosol depending on the relative humidity of the air overlaying the cloud. Wang et al. (2003) showed that all else being equal, polluted stratocumulus clouds tend to have lower water contents than clean clouds because the small droplets associated with polluted clouds evaporate more readily and induce an evaporation-entrainment feedback that dilutes the cloud. This result was confirmed by Xue and Feingold (2006) and Jiang and Feingold (2006) for shallow cumulus, where pollution particles were shown to decrease cloud fraction. Furthermore, Xue et al. (2007) suggested that there may exist two regimes: the first, a precipitating regime at low aerosol concentrations where an increase in aerosol will suppress precipitation and increase cloud cover (Albrecht, 1989); and a second, non precipitating regime where the enhanced evaporation associated with smaller drops will decrease cloud water and cloud fraction.

Finally, the question of possible effects of aerosol on cloud lifetime was examined by Jiang et al. (2006) who tracked hundreds of cumulus clouds generated by LES from their formative stages until they dissipated. They showed there was no effect of aerosol on cloud lifetime, and that cloud lifetime was dominated by dynamical variability.

It could be argued that the representation of these complex feedbacks in GCMs is not warranted until a better understanding of the processes is at hand. Moreover, until GCMs are able to represent cloud scales, it is questionable what can be obtained by adding microphysical complexity to poorly resolved clouds. A better representation of aerosol-cloud interactions in GCMs therefore depends on our ability to improve representation of aerosols and clouds, as well as their interaction. We return to this discussion in the next chapter.

## 3.4. Impacts of Aerosols on Model Climate Simulations

It was noted in the introduction that aerosol cooling is essential in order for models to produce the observed global temperature rise over the last century, at least models with climate sensitivities in the range of 3°C for doubled $CO_2$ (or ~0.75°C/$Wm^{-2}$). Here we discuss this in somewhat more detail.

Hansen et al. (2007) show that in the GISS model well-mixed greenhouse gases produce a warming of close to 1°C between 1880 and the present {**Table 3.5** adapted from Hansen et al., 2007 Table 1}. The direct effect of tropospheric aerosols as calculated in that model produces cooling of close to –0.3°C between those same years, while the indirect effect (represented in that study as cloud cover change) produces an additional cooling of similar magnitude [note that in contrast, in the general model result quoted in IPCC (2007), the radiative forcing from indirect aerosols is twice that of the direct effect].

The time dependence of the total aerosol forcing as well as the individual species components is shown in **Figure 3.21** {adapted from Hansen et al., 2007 Fig.3c}. The resultant warming, of ~0.5°C including these and other forcings (Table 3.5), is less than observed. Hansen et al. (2007) further show that a reduction in sulfate optical thickness and the direct aerosol effect by 50%, which also reduced the aerosol indirect effect by 18%, results in the aerosol negative forcing from 1880 to 2003 being –0.91 $Wm^{-2}$ (down from –1.37 $Wm^{-2}$ with this revised forcing). The model now warms 0.75°C over that time period, closer to the observed warming of 0.8°C. Hansen et al. (op cit.) defend this change by noting that sulfate aerosol removal over North America and western Europe during the 1990s led to a cleaner atmosphere. Note that the comparisons shown in the previous section suggest that the GISS model already underestimates aerosol optical depths; it is thus trends that are the issue here.

**Table 3.5.** Climate forcings (1880-2003) used to drive GISS climate simulations, along with the surface air temperature changes obtained for several periods. Instantaneous (Fi), adjusted (Fa), fixed SST (Fs) and effective (Fe) forcings are defined in Hansen et al. 2005. From Hansen et al., 2007.

| **Forcing Agent** | **Forcing $Wm^{-2}$ (1880-2003)** | | | | **ΔT surf °C [Year to 2003]** | | | |
|---|---|---|---|---|---|---|---|---|
| | **Fi** | **Fa** | **Fs** | **Fe** | **1880** | **1900** | **1950** | **1979** |
| Well-mixed GHGs | 2.62 | 2.50 | 2.65 | 2.72 | .96 | .93 | .74 | .43 |
| Stratospheric $H_2O$ | - | - | .06 | .05 | .03 | .01 | .05 | .00 |
| Ozone | .44 | .28 | .26 | .23 | .08 | .05 | .00 | -.01 |
| Land Use | - | - | -.09 | -.09 | -.05 | -.07 | -.04 | -.02 |
| Snow Albedo | .05 | .05 | .14 | .14 | .03 | .00 | .02 | -.01 |
| Solar Irradiance | .23 | .24 | .23 | .22 | .07 | .07 | .01 | .02 |
| Strat Aerosols | .00 | .00 | .00 | .00 | -.08 | -.03 | -.06 | .04 |
| Trop. Aer., Direct | -.41 | -.38 | -.52 | -.60 | -.28 | -.23 | -.18 | -.10 |
| Trop. Aer., 2nd IE | - | - | -.87 | -.77 | -.27 | -.29 | -.14 | -.05 |
| **Sum of Above** | **-** | **-** | **1.86** | **1.9** | **.49** | **.44** | **.40** | **.30** |
| **All Forcings at once** | **-** | **-** | **1.77** | **1.75** | **.53** | **.61** | **.44** | **.29** |

This is not the only example of inverse-reasoning (Anderson et al., 2003), in which model simulations incorporate aerosols calibrated to bring the temperature change results closer to observations. The magnitude of the indirect effect, as discussed by Hansen et al. (2005) is roughly tuned to produce the required response. The authors justify this approach by claiming that paleoclimate data indicate a climate sensitivity of close to 0.75°(±0.25) C/Wm$^{-2}$, and therefore something close to this magnitude of negative forcing is reasonable. Even this stated range leaves significant uncertainty in climate sensitivity and the magnitude of the aerosol negative forcing. Furthermore, IPCC (2007) concluded that paleoclimate data is *not* capable of narrowing the range of climate sensitivity, nominally 0.375 to 1.13 °C/Wm$^{-2}$, because of uncertainties in paleoclimate forcing and response, so from this perspective the total aerosol forcing is even less constrained than the GISS estimate. Hansen et al. (2007) acknowledge that (in their words) "an equally good match to observations probably could be obtained from a model with larger sensitivity and smaller net forcing, or a model with smaller sensitivity and larger forcing".

The GFDL model results for global mean ocean temperature change (down to 3 km depth) for the time period 1860 to 2000 is shown in **Figure 3.22** {adapted from Delworth et al., 2005, Fig. 1}, along with the different contributing factors (Delworth et al., 2005). This is the same GFDL model whose aerosol distribution was discussed previously. The aerosol forcing produces a cooling on the order of 50% that of greenhouse warming (generally similar to that calculated by the GISS model, Table 3.5). Similar reasoning concerning the somewhat arbitrary nature of the aerosol forcing applies to this model conclusion, in particular concerning the indirect aerosol cooling.

The general model response noted by IPCC, as discussed in the introduction, was that the total aerosol effect of –1.2 Wm$^{-2}$ reduced the greenhouse forcing of some 3 W m$^{-2}$ by about 40%, in the neighborhood of the GFDL and GISS forcings. Since the average model sensitivity was close to 0.75 Wm$^{-2}$,

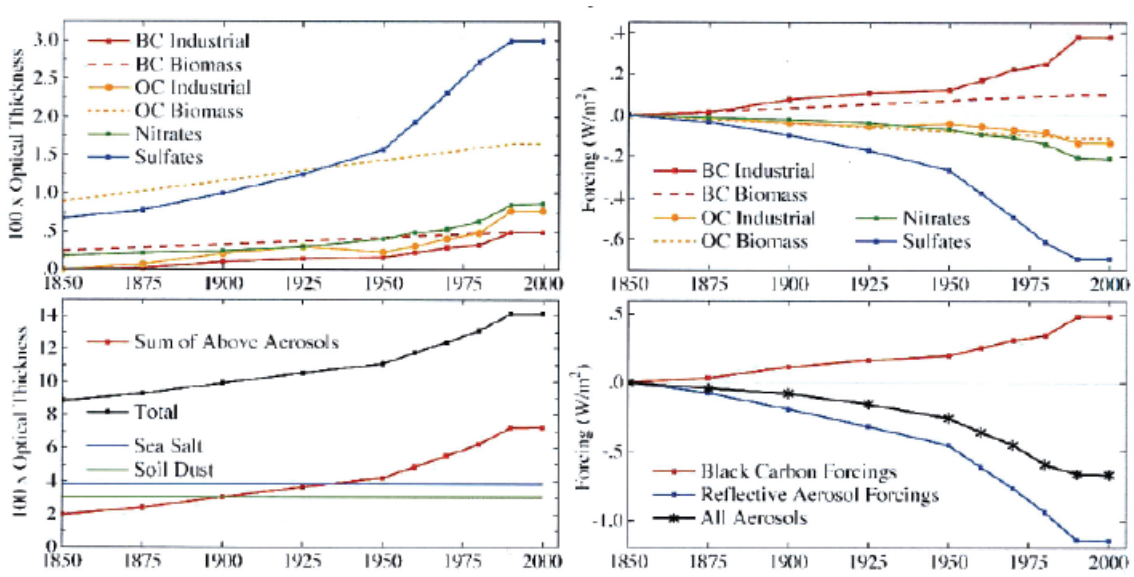


**Fig. 3.21.** Time dependence of aerosol optical thickness (left) and effect climate forcing (right). Note that as specified, the aerosol trends are all 'flat' from 1990 to 2000. From Hansen et al. (2007).

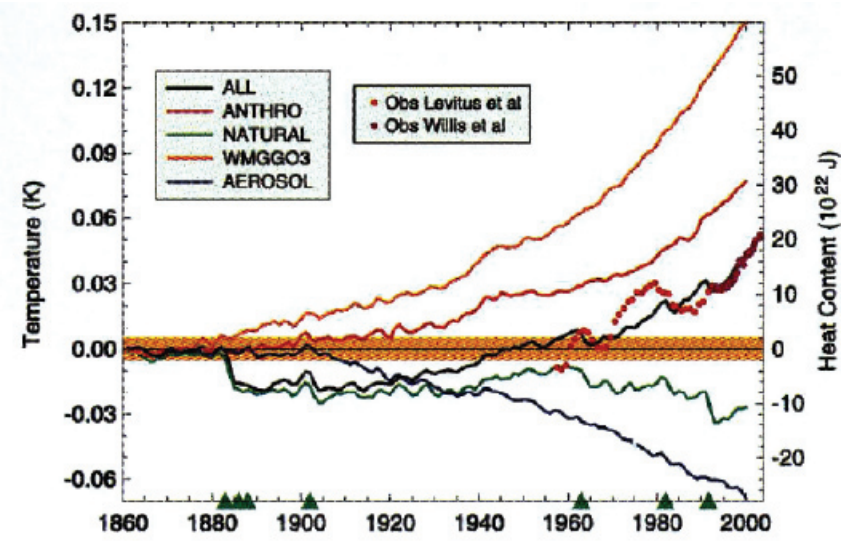


**Fig. 3.22.** Change in global mean ocean temperature (left axis) and ocean heat content (right axis) for the top 3000 m due to different forcings in the GFDL model. WMGG includes all greenhouse gases and ozone; NATURAL includes solar and volcanic aerosols (events shown as green triangles on the bottom axis). Observed ocean heat content changes are shown as well. From Delworth et al., 2005.

similar to the sensitivities of these models, the necessary negative forcing is therefore similar. The agreement cannot therefore be used to validate the actual aerosol effect until climate sensitivity itself is better known.

Is there some way to distinguish between greenhouse gas and aerosol forcing that would allow the observational record to indicate how much of each was really occurring? This question of attribution has been the subject of numerous papers, and the full scope of the discussion is beyond the range of this report. It might be briefly noted that Zhang et al. (2006) using results from several GCMs and including both spatial and temporal patterns, found that the climate responses to greenhouse gases and sulfate aerosols are correlated, and separation is possible only occasionally, especially at global scales and during summer when the aerosol effect on solar absorption is likely to be bigger. The conclusions concerning this appear to be model and method-dependent: using time-space distinctions as opposed to trend detection may work differently in different models (Gillett et al., 2002a). Using multiple models helps primarily by providing larger-ensemble sizes for statistics (Gillett et al., 2002b). However, even distinguishing between the effect of different aerosol types is difficult. Jones et al. (2005) concluded that currently the pattern of temperature change due to black carbon is indistinguishable from the sulfate aerosol pattern. In contrast, Hansen et al. (2005) found that absorbing aerosols produce a different global response than other forcings, and so may be distinguishable. Overall, the similarity in response to all these very different forcings is undoubtedly due to the importance of climate feedbacks in amplifying the forcing, whatever be its nature.

Distinctions in the climate response do appear to arise in the vertical, where absorbing aerosols produce warming that is exhibited throughout the troposphere and into the stratosphere, whereas reflective aerosols cool the troposphere but warm the stratosphere (Hansen et al., 2005). Delworth et al. (2005) noted that in the ocean, the cooling effect of aerosols extended to greater depths, due to the thermal instability associated with cooling the ocean surface. Hence the temperature response at levels both above and below the surface may provide an additional constraint on the magnitudes of each of these forcings.

## 3.5. Implications of comparisons of modeled and observed aerosols for climate model simulations.

The comparisons in subsections 2 and 3 suggest (tentatively) that models may underestimate aerosol concentrations and the direct effect over the oceans and in the Southern Hemisphere, and over land in the tropics, while overestimating it over land in the Northern Hemisphere. If so, the global average response would be more accurate than the hemispheric differentiation. The fact that the total optical depth is in better agreement between models than the individual components means that even with similar optical depths, the aerosol direct forcing effect may be quite different (as it is in the difference models, e.g., Fig. 3.12).

The indirect effect is strongly influenced by the aerosol concentrations, so if the above discrepancies are true, the indirect effect will also have these shortcomings. If that proves to be the case, than the model simulations of anthropogenic warming over land in the Northern Hemisphere would be underestimated (aerosol cooling being too large), while the warming is overestimated in other regions. It is, however, important to distinguish between those aerosols that are expected to change with time and those that are not; model discrepancies concerning the latter category will not affect the climate change simulations nearly as strongly. And errors in absorbing aerosols (e.g., black carbon) will have somewhat of an opposite climate influence from errors in reflecting aerosols (e.g., sulfates).

This type of speculation can only be better quantified when aerosol observations and models are improved. The pathway to this objective is discussed in the following chapter.

**References**

**Ackerman**, A. S., M. P. Kirkpatrick, D. E. Stevens and O. B. Toon, 2004: The impact of humidity above stratiform clouds on indirect aerosol climate forcing. *Nature*, **432**, 1014-1017.

**Albrecht**, B. 1989: Aerosols, cloud microphysics and fractional cloudiness. *Science*, **245**, 1227-1230.

**Anderson**, T. L., R. J. Charlson, S. E. Schwartz, R. Knutti, O. Boucher, H. Rodhe and J. Heintzenberg, 2003: Climate forcing by aerosols – a hazy picture. *Science*, **300**, 1103-1104.

**Andreae**, M. O., D. Rosenfeld, P. Artaxo, A. A. Costa, G. P. Frank, K. M. Longo and M. A. F. Silvas-Dias, 2004: Smoking rain clouds over the amazon. *Science*, **303**, 1337-1342.

**Bates**, T. S. et al., 2006: Aerosol direct radiative effects over the northwest Atlantic, northwest Pacific, and North Indian Oceans: estimates based on in-situ chemical and optical measurements and chemical transport modeling. *Atmos. Chem. Phys. Discuss.*, **6**, 175-362.

**Boucher**, O., and M. Pham, 2002: History of sulfate aerosol radiative forcings. *Geophys. Res. Lett.*, **29**, 22–25.

**Chin**, M. et al., 2002: Tropospheric aerosol optical depth from the GOCART model and comparisons with satellite and Sun photometer measurements. *J. Atmos. Sci.*, **59**, 461-483.

**Chung**, C. E. and G. Zhang, 2004: Impact of absorbing aerosol on precipitation. *J.* Geophys. *Res.*, **109**, doi:10.1029/2004JD004726.

**Coakley**, J. A. Jr. and C. D. Walsh, 2002: Limits to the Aerosol Indirect Radiative Effect Derived from Observations of Ship Tracks. *J. Atmos. Sci.*, **59**, 668-680

**Delworth**, T. L., V. Ramaswamy and G. L. Stenchikov, 2005: The impact of aerosols on simulated ocean temperature and heat content in the 20th century. *Geophys. Res. Lett.*, **32**, doi:10.1029/2005GL024457.

**Dusek**, U., G. P. Frank, L. Hildebrandt, J. Curtius, S. Walter, D. Chand, F. Drewnick, S. Hings, D. Jung, S. Borrmann, and M. O. Andreae (2006), Size matters more than chemistry in controlling which aerosol particles can nucleate cloud droplets, *Science*, *312*, 1375-1378.

**Eagan**, R. c., P. V. Hobbs and L. F. Radke, 1974: Measurements of cloud condensation nuclei and cloud droplet size distributions in the vicinity of forest fires. *J. Appl. Meteor.*, **13**, 553-557.

**Ervens**, B., G. Feingold, and S. M. Kreidenweis, 2005: The influence of water-soluble organic carbon on cloud drop number concentration. *J. Geophys. Res.*, **110,** D18211, doi:10.1029/2004JD005634.

**Feingold**, G., B. Stevens, W.R. Cotton, and R.L. Walko, 1994: An explicit microphysics/LES model designed to simulate the Twomey Effect. *Atmospheric Research*, **33**, 207-233.

**Feingold**, G., W. R. Cotton, S. M. Kreidenweis, and J. T. Davis, 1999: Impact of giant cloud condensation nuclei on drizzle formation in marine stratocumulus: Implications for cloud radiative properties. *J. Atmos. Sci.*, **56**, 4100-4117.

**Feingold**, G., 2003: Modeling of the first indirect effect: Analysis of measurement requirements. *Geophys. Res. Lett.*, **30**, No. 19, doi:10.1029/2003GL017967.

**Feingold**, G., H. Jiang, and J. Y. Harrington, 2005: On smoke suppression of clouds in Amazonia. *Geophys. Res. Lett.*, **32**, No. 2, L02804, 10.1029/2004GL021369.

**Fitzgerald**, J. W., 1975: Approximation formulas for the equilibrium size of an aerosol particle as a function of its dry size and composition and the ambient relative humidity, *J. Appl. Meteor.* **14**, 1044-1049.

**Gillett**, N.P., et al., 2002a: Reconciling two approaches to the detection of anthropogenic influence on climate. *J. Clim.*, **15**, 326–329.

**Gillett**, N.P., et al., 2002b: Detecting anthropogenic influence with a multimodel ensemble. *Geophys. Res. Lett.*, **29,** doi:10.1029/2002GL015836.

**Ginoux**, P., M. Chin, I. Tegen, J. M. Prospero, B. Holben, O. Dubovik and S.-J. Lin, 2001: Sources and distributions of dust aerosols simulated with the GOCART model. *J. Geophys. Res.*, **20**, 20255-20273.

**Ginoux**, P., L. W. Horowitz, V. Ramaswamy, I. V. Geogdzhayev, B. N. Holben, G. Stenchikov and X. Tie, 2006: Evaluation of aerosol distribution and optical depth in the Geophysical Fluid Dynamics Laboratory coupled model CM2.1 for present climate. *J. Geophys. Res.*, **111**, doi:10.1029/2005JD006707.

**Golaz**, J-C., V. E. Larson, and W. R. Cotton, 2002a: A PDF-based model for boundary layer clouds. Part I: Method and model description, *J. Atmos. Sci*., **59**, 3540-3551.

**Golaz**, J-C., V. E. Larson, and W. R. Cotton, 2002b: A PDF-based model for boundary layer clouds. Part II: Model results. *J. Atmos. Sci*., **59**, 3552-3571.

**Grabowski**, W.W., 2004: An improved framework for superparameterization. *J. Atmos. Sci*., **61**, 1940-52.

**Grabowski**, W.W., X. Wu, and M.W. Moncrieff, 1999: Cloud resolving modeling of tropical cloud systems during Phase III of GATE. Part III: Effects of cloud microphysics, *J. Atmos. Sci*., **56**, 2384-2402.

**Gregory**, J.M., et al., 2002: An observationally based estimate of the climate sensitivity. *J. Clim.*, **15,** 3117–3121.

**Han**, Q. Y., W. B. Rossow, J. Zeng, and R. M. Welch, 2002: Three different behaviors of liquid water path of water clouds in aerosol-cloud interactions. *J. Atmos. Sci.*, **59**, 726-735.

**Hansen**, J., M. Sato and R. Ruedy, 1997: Radiative forcing and climate response. *J. Geophys. Res.*, **102**, 6831-6864.

**Hansen**, J., et al., 2005: Efficacy of climate forcings. *J. Geophys. Res.*, **110**, doi:10.1029/2005JD005776, 45pp.

**Hansen**, J. et al., 2007: Climate simulations for 1880-2003 with GISS model E. *J. Geophys. Res.*, in press.

**Harvey**, L.D.D., 2004: Characterizing the annual-mean climatic effect of anthropogenic $CO_2$ and aerosol emissions in eight coupled atmosphere-ocean GCMs. *Clim. Dyn.,* **23**, 569–599.

**IPCC**, 2007: Climate Change 2007: *The Physical Science Basis. Contribution of Working Group I to the Fourth Assessment Report of the Intergovernmental Panel on Climate Change* [Solomon, S., D. Qin, M. Manning, Z. Chen, M. Marquis, K.B. Avery, M. Tignor and H.L. Miller (eds.)]. Cambridge University Press, Cambridge, United Kingdom and New York, NY, USA, 996 pp.

**Jiang**, H., and G. Feingold, 2006: Effect of aerosol on warm convective clouds: Aerosol-cloud-surface flux feedbacks in a new coupled large eddy model. *J. Geophys. Res.*, **111**, D01202, doi:10.1029/2005JD006138.

**Jiang**, H., H. Xue, A. Teller, G. Feingold, and Z. Levin, 2006: Aerosol effects on the lifetime of shallow cumulus. *Geophys. Res. Lett.*, **33**, doi: 10.1029/2006GL026024.

**Jones**, G.S., et al., 2005: Sensitivity of global scale attribution results to inclusion of climatic response to black carbon. *Geophys. Res. Lett.*, **32**, L14701, doi:10.1029/2005GL023370.

**Kaufman**, Y. J., I. Koren, L. A. Remer, D. Rosenfeld and Y. Rudich, 2005: The effect of smoke, dust and pollution aerosol on shallow cloud development over the Atlantic Ocean. *Proc. Natl. Acad. Sci.*, **102**, 11207-11212.

**Kerr**, R., 2007: Another global warming icon comes under attack. *Science*, **317**, 28.

**Kiehl**, J. T., 2007: Twentieth century climate model response and climate sensitivity. *Geophys. Res. Lett.*, **34**, doi:10.1029/2007GL031383.

**Kinne**, S., et al., 2006: An AeroCom initial assessment: optical properties in aerosol component modules of global models. *Atmos. Chem. Phys*. **6**, 1815–1834.

**Knutti**, R., T.F. Stocker, F. Joos, and G.-K. Plattner, 2002: Constraints on radiative forcing and future climate change from observations and climate model ensembles. *Nature,* **416,** 719–723.

**Knutti**, R., T.F. Stocker, F. Joos, and G.-K. Plattner, 2003: Probabilistic climate change projections using neural networks. *Clim. Dyn.*, **21**, 257– 272.

**Koch**, D., 2001: Transport and direct radiative forcing of carbonaceous and sulfate aerosols in the GISS GCM. *J. Geophys. Res.*, **106**, 20311-20332.

**Koch**, D., G. A. Schmidt and C. V. Field, 2006: Sulfur, sea salt and radionuclide aerosols in GISS Model E. *J. Geophys. Res.*, **111**, doi:10.1029/2004JD005550.

**Kogan**, Y. L., D. K. Lilly, Z. N. Kogan, and V. Filyushkin, 1994: The effect of CCN regeneration on the evolution of stratocumulus cloud layers. *Atmos. Res.*, **33**, 137- 150.

**Kruger**, O. and Grasl, H., 2002: The indirect aerosol effect over Europe. *Geophys. Res. Lett.*, **29**, doi:10.1029/2001GL014081.

**Larson**, V. E., R. Wood, P. R. Field, J.-C. Golaz, T. H. Vonder Haar, and W. R. Cotton, 2001: Small-scale and mesoscale variability of scalars in cloudy boundary layers: One-dimensional probability density functions, *J. Atmos. Sci*., **58**, 1978-1996.

**Larson**, V.E., J.-C. Golaz, H. Jiang and W.R. Cotton, 2005: Supplying local microphysics parameterizations with information about subgrid variability: Latin hypercube sampling, *J. Atmos. Sci.*, **62,** 4010-4026.

**Lefohn**, A. S., J. D. Husar and R. B. Husar, 1999: Estimating historical anthropogenic global sulfur emission patterns for the period 1850-1990. *Atm. Env.*, **33**, 3435-3444.

**Liousse**, C., J. E. Penner, C. Chuang, J. J. Walton, H. Eddleman and H. Cachier, 1996: A three-dimensional model study of carbonaceous aerosols. *J. Geophys. Res.*, **101**, 19411-19432.

**Liu**, L., A. A. Lacis, B. E. Carlson, M. I. Mishchenko, and B. Cairns, 2006: Assessing Goddard Institute for Space Studies ModelE aerosol climatology using satellite and ground-based measurements: A comparison study. *J. Geophys. Res.*, **111**, doi:10.1029/2006JD007334.

**Lohmann**, U., J. Feichter, C. C. Chuang, and J. E. Penner, 1999: Prediction of the number of cloud droplets in the ECHAM GCM, *J. Geophys. Res.*, **104**, 9169-9198.

**Lohmann**, U. and J. Feichter, 2005: Global indirect aerosol effects: a review. *Atmos. Chem. Phys.*, **5**, 715-737.

**Lohmann**, U., I. Koren and Y.J. Kaufman, 2006: Disentangling the role of microphysical and dynamical effects in determining cloud properties over the Atlantic, *Geophys. Res. Lettr.,* **33**, L09802.

**McFiggans**, G., P. Artaxo, U. Baltensberger, H. Coe, M.C. Facchini, G. Feingold, S. Fuzzi, M. Gysel, A. Laaksonen, U. Lohmann, T. F. Mentel, D. M. Murphy, C. D. O'Dowd, J. R. Snider, E. Weingartner, 2006: The effect of physical and chemical aerosol properties on warm cloud droplet activation. *Atmos. Chem. Phys.*, **6**, 2593-2649.

**Menon**, S., A.D. Del Genio, Y.J. Kaufman, R. Bennartz, D. Koch, N. Loeb and D. Orlikowski, 2007: Analyzing signatures of aerosol-cloud interactions from satellite retrievals and the GISS GCM. J. Geophys. Res., In Review.

**Mishchenko**, M. I. And I. V. Geogdzhayev, 2007: GACP data show potential climate impact of aerosols. *GEWEX*, **17**, 4-5.

**Nakicenovic**, N. et al., 2000: *Special Report on Emissions Scenarios: A Special Report of Working Group III of the Intergovernmental Panel on Climate Change*, Cambridge University Press, Cambridge, U.K., 599 pp.

**Penner**, J. E. et al., 2002: A comparison of model- and satellite-derived aerosol optical depth and reflectivity. *J. Atmos. Sci.*, **59**, 441-460.

**Penner**, J. E., et al. 2006: Model intercomparison of indirect aerosol effects. *Atmos. Chem. Phys., Discuss.*, **6**, 1579-1617.

**Pincus**, R., and S.A. Klein, 2000: Unresolved spatial variability and microphysical process rates in large-scale models, *J. Geophys. Res.*, **105**, 27,059-27,065.

**Quaas**, J., O. Boucher and U. Lohmann, 2006: Constraining the total aerosol indirect effect in the LMDZ GCM and ECHAM4 GCMs using MODIS satellite data. *Atmos. Chem. Phys. Disc.,* **5**, 9669-9690.

**Ramanathan**, V., P. J. Crutzen, J. T. Kiehl and D. Rosenfeld, 2001: Aerosols, climate and the hydrological cycle. *Science*, **294**, 2119-2124.

**Randall**, D., M. Khairoutdinov, A. Arakawa, and W. Grabowski, 2003: Breaking the cloud parameterization deadlock, *Bull. Amer. Meteorol. Soc.*, **84**, 1547-1564.

**Reddy**, M. S., O. Boucher, N. Bellouin, M. Schulz, Y. Balkanski, J.-L. Dufresne and M. Pham, 2005: Estimates of global multicomponent aerosol optical depth and radiative perturbation in the Laboratoire de Meteorologie Dynamique general circulation model. *J/ Geophys. Res.*, **110**, doi:10.1029/2004JD004757.

**Rissler**, J., E. Swietlicki, J. Zhou, G. Roberts, M. O. Andreae, L. V. Gatti, and P. Artaxo 2004: Physical properties of the sub-micrometer aerosol over the Amazon rain forest during the wet-to-dry season transition – comparison of modeled and measured CCN concentrations, *Atmos. Chem. Phys.,* **4**, 2119-2143.

**Roderick**, M. L. and G. D. Farquhar, 2002: The cause of decreased pan evaporation over the past 50 years. *Science*, **298**, 1410-1411.

**Rosenfeld**, D., 2000: Suppression of rain and snow by urban and industrial air pollution. *Science,* **287**, 1793-1796.

**SAP** 1.1, 2006: Temperature Trends in the Lower Atmosphere. T. R. Karl, S. J. Hassol, C. D. Miller and W. L. Murray, editors. Available from the Global Change Research Information Office, Washington, D.C. 164pp.

**Schmidt**, G. A., et al., 2006: Present-day atmospheric simulations using GISS Model E: Comparison to in-situ, satellite and reanalysis data. *J. Clim.*, **19**, 153-192.

**Schulz**, M. et al., 2006: Radiative forcing by aerosols as derived from the AeroCom present-day and pre-industrial simulations. *Atmos. Chem. Phys*., **6**, 5225–5246.

**Schwartz**, S. E., R. J. Charlson and H. Rodhe, 2007: Quantifying climate change – too rosy a picture? *Nature Reports*, *Climate Change*, **2**, 23-24.

**Smith**, S.J., Pitcher, H. and Wigley, T.M.L., 2001: Global and regional anthropogenic sulfur dioxide emissions. *Global and Planetary Change* 29, 99- 119.

**Sotiropoulou**, R.E.P, Nenes, A., Adams, P.J., Seinfeld, J.H. (2007) Cloud condensation nuclei prediction error from application of Kohler theory: Importance for the aerosol indirect effect, *J.Geoph. Res.*, **112**, D12202, doi:10.1029/2006JD007834

**Sotiropoulou**, R.E.P, Medina, J., Nenes A. (2006) CCN predictions: is theory sufficient for assessments of the indirect effect?, *Geoph.Res.Let.*, **33**, L05816, doi:10.1029/2005GL025148

**Stevens**, B., G. Feingold, R. L. Walko and W. R. Cotton, 1996: On elements of the microphysical structure of numerically simulated non-precipitating stratocumulus. J. Atmos. Sci., 53, 980-1006.

**Storlevmo**, T., J.E. Kristjansson, G. Myhre, M. Johnsud, and F. Stordal, 2006: Combined observational and modeling based study of the aerosol indirect effect, *Atmos. Chem. Phys. Dis*., **6**, 3757-3799.

**Stott**, P.A., et al., 2006: Observational constraints on past attributable warming and predictions of future global warming. *J. Clim.*, **19**, 3055– 3069.

**Textor**, C., et al., 2007: The effect of harmonized emissions on aerosol properties in global models - an AeroCom experiment. *Atmos. Chem.Phys. D*isc., 2007.

**Tie**, X. et al., 2005: Assessment of the global impact of aerosols on tropospheric oxidants. *J. Geophys. Res.*, **110**, doi:10.1029/2004JD005359.

**Twomey**, S. A., 1977: The influence of pollution on the shortwave albedo of clouds. *J. Atmos. Sci.*, **34**, 1149-1152.

**Van Ardenne**, J. A., Dentener, F. J., Olivier, J. G. J., Klein, Goldewijk, C. G. M., and Lelieveld, J., 2001: A 1° x 1° resolution data set of historical anthropogenic trace gas emissions for the period 1890–1990. *Global Biogeochem. Cycl*. **15**, 909–928.

**Wang**, S., Q. Wang, and G. Feingold, 2003: Turbulence, condensation and liquid water transport in numerically simulated nonprecipitating stratocumulus clouds. *J. Atmos. Sci.*, **60**, 262-278.

**Warner**, J., 1968: A reduction of rain associated with smoke from sugar-cane fires—An inadvertent weather modification, *J. App. Meteor.,* **7**, 247–251.

**Wen**, G., A. Marshak, R. F. Cahalan, L. A. Remer, R. G. Kleidman, 2007: 3-D aerosol cloud radiative interaction observed in collocated MODIS and ASTER images of cumulus cloud fields. J. Geophys. Res., 112, No, D13, D1320410.1029/2006JD008267

**Wild**, M., et al., 2005: From dimming to brightening: decadal changes in solar radiation at Earth's surface. *Science*, **308**, 847-850.

**Xue**, H., G. Feingold, and B. Stevens, 2007: Aerosol effects on clouds, precipitation, and the organization of shallow cumulus convection. *J. Atmos. Sci.*, in press.

**Xue**, H., and G. Feingold, 2006: Large eddy simulations of trade-wind cumuli: Investigation of aerosol indirect effects. *J. Atmos. Sci.*, **63**, 1605-1622.

**Yu H.**, S. C. Liu, and R. E. Dickinson, 2002: Radiative effects of aerosols on the evolution of the atmospheric boundary layer, *J. Geophys. Res.*, **107** (D12), doi:10.1029/2001JD000754.

**Zhang**, X., F.W. Zwiers, and P.A. Stott, 2006: Multi-model multi-signal climate change detection at regional scale. *Journal of Climate,* **19**, 4294-4307.

**Appendix A.1**

An approximate relation between aerosol optical depth and aerosol mass loading may be developed as follows. The local mass concentration for a single particulate component of an aerosol is given as an integral over size distribution as

$$m = \frac{4\pi\rho}{3}\int r^3 n(r)\,dr \tag{1}$$

where is the size distribution of the aerosol normalized such that $\int n(r)dr = N$ where $N$ is the total number concentration. For multiple aerosol species

$$m = \sum m_i = \frac{4\pi}{3}\int r^3 [\sum \rho_i(r) n_i(r)]dr = \frac{4\pi}{3}\sum \rho_i \int r^3 n_i(r)dr \tag{2}$$

where the latter equality holds if the density of the individual aerosol species is independent of radius, a good approximation for particles sufficiently large to contribute appreciably to mass concentration. Finally the column mass burden (amount of aerosol particulate matter per Earth surface area) is

$$M = \int m(z)\,dz = \frac{4\pi}{3}\int\left\{\sum \rho_i(z)\int r^3 n_i(r,z)\,dr\right\}dz \tag{3}$$

where the dependence of particle size and density on height $z$ is explicitly noted; such dependence is to be expected both through the intrinsic dependence of aerosol loading on height that results from prior mixing and transformation processes, and through the dependence relative humidity with height and the dependence of particle size on relative humidity (which can be quite strong, especially for high relative humidity as might be encountered near the top of the boundary layer). This mass burden can in turn be expressed in terms of a weighted average density of the aerosol in the column $\langle\rho\rangle$ as

$$M = \frac{4\pi}{3}\langle\rho\rangle\int\left\{\int r^3 n(r)\,dr\right\}dz \tag{4}$$

where

$$\langle \rho \rangle = \frac{\int \{ \sum \rho_i(z) \int r^3 n_i(r,z) dr \} dz}{\int \{ \int r^3 n(r) dr \} dz} \tag{5}$$

Similarly the local extinction coefficient of the aerosol particulate matter is given for a single component aerosol as

$$\sigma_{ep}(\lambda) = \int r^2 Q_e(r,\lambda) n(r) dr \tag{6}$$

where $Q_e$ ($r$, $\lambda$) is the extinction efficiency factor, a function of particle size, composition (through index of refraction) and wavelength. The extinction coefficient is related to the phase function and the single scattering albedo of the aerosol. Again for a multicomponent aerosol

$$\sigma_{ep}(\lambda) = \sum \sigma_{ep,\,i}(\lambda) = \sum \int r^2 Q_{e,\,i}(r,\lambda)\, n_i(r)\, dr \tag{7}$$

Finally the aerosol optical depth is given as the integral of extinction coefficient with height:

$$\tau(\lambda) = \int \sigma_{ep}(\lambda, z)\, dz = \sum \{ \int r^2 Q_{e,\,i}(r,\lambda,z)\, n_i(r,z) dr \} \tag{8}$$

where the extinction efficiency implicitly depends on height through the dependence of index of refraction on composition, which even for a single component aerosol will vary with varying relative humidity through the dependence of index of refraction on water content of the particulate matter. This wavelength dependent optical depth can in turn be expressed in terms of a weighted average scattering efficiency in the column (also wavelength dependent) $\langle Q_e(\lambda) \rangle$ as

$$\tau(\lambda) = \langle Q_e(\lambda) \rangle \int \{ \int r^2 n(r) dr \} dz \tag{9}$$

where

$$\langle Q_e(\lambda) \rangle = \frac{\sum \{ \int r^2 Q_{e,\,i}(r,\lambda,z) n_i(r,z)\, dr \}}{\int \{ \int r^2 n(r)\, dr \} dz} \tag{10}$$

Hence the aerosol optical depth is related to the column mass burden as

$$\tau(\lambda) = \frac{3 \langle Q_e(\lambda) \rangle M}{4\pi \langle \rho \rangle r_{eff}} \tag{11}$$

where the effective radius $r_{eff}$ is given by its usual definition (ratio of third to second moments of the distribution; Hansen and Travis, 1974) integrated over the aerosol column as

$$r_{eff} = \frac{\int \{ \int r^3 n(r) dr \} dz}{\int \{ \int r^2 n(r) dr \} dz} \tag{12}$$

and is an intensive aerosol property that is related to the Ångström exponent.

**Appendix A.2**

Several recent studies have pointed to formation of secondary organic aerosol in amounts and at rates that cannot be accounted for in current chemical modeling. In aircraft measurements in urban-influenced air in New England DeGouw et al (2005) found that particulate organic matter (POM) was highly correlated with secondary anthropogenic gas-phase species, strongly suggesting that the POM derived from secondary anthropogenic sources. This is illustrated in **Figure A2.1**, which shows scatterplots of submicrometer POM versus acetylene (a primary emitted species) and isopropyl nitrate (a secondary organic species formed by atmospheric reactions of primary emitted species) The increase in submicrometer POM with increasing photochemical age could not be explained by the removal of aromatic precursors alone, suggesting that other species must have contributed and/or that the mechanism for POM formation is more efficient than previously assumed.

A further example is aerosol production in Mexico City, **Figure A2.2**, that showed amounts of secondary organic aerosol (SOA) produced from anthropogenic volatile organic carbon at rates as much as

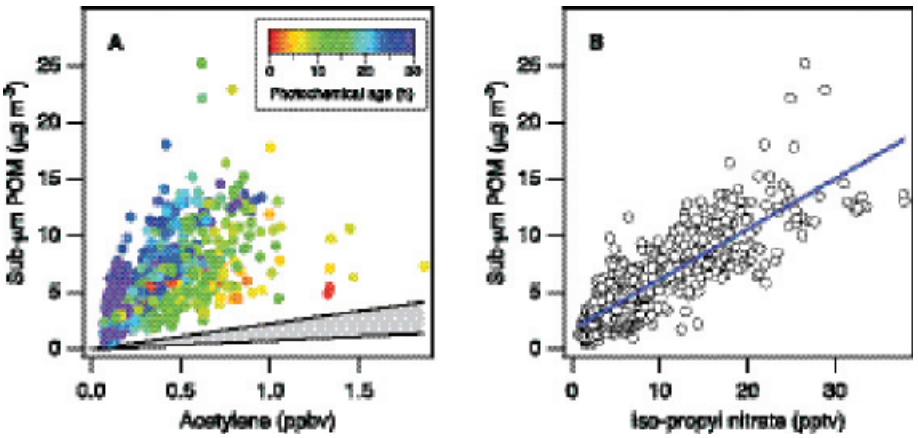


**Figure A2.1.** Scatterplots of the submicrometer particulate organic matter (POM) measured during the 1992 New England Air Quality Study versus (a) acetylene and (b) isopropyl nitrate. The colors of the data points in a denote the photochemical age as determined by the ratios of compounds of known OH reactivity; the gray area shows the range of ratios between submicrometer POM and acetylene typical of urban air. Modified from De Gouw et al. (2006).

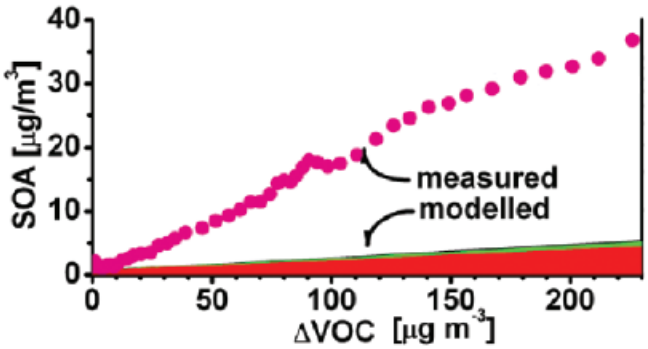


**Figure A2.2.** Measured and modeled secondary organic aerosol (SOA) formation in Mexico City on April 9 2003. Comparison of measured and modeled concentration of secondary organic aerosol SOA versus concentration of volatile organic carbon VOC calculated to have been oxidized. Shaded areas indicate the calculated amount of SOA-mass concentration attributed to aromatics (red), alkenes (green), alkanes (black). Modified from Volkamer et al (2006).

eight-fold greater than predicted by current models. Also contrary to current understanding, much of the excess secondary organic aerosol is formed from first-generation oxidation products.

The production of organic aerosol downwind of Mexico City has been further examined more recently in aircraft studies by normalizing the aerosol to carbon monoxide to account for dilution. Aerosol composition was determined by mass spectrometry, which showed the increasing dominance of the organic component of the aerosol over roughly one day of photochemical processing, **Figure A2.3**. The measured increase in organic aerosol exceeded the modeled increase, based on laboratory experiments and measured volatile organic carbon, by an order of magnitude.

The amount of organic aerosol formed by atmospheric reactions can be much greater than expected on the basis of present photochemical models, which are derived from theory and laboratory experiments. Aircraft measurements of organic carbon aerosol over the northwest Pacific revealed unexpectedly high concentrations in the free troposphere (FT) 10–100 times higher than computed with a global chemical transport model including a standard simulation of secondary organic aerosol formation based on empirical fits to smog chamber data. The same model was able to reproduce the observed vertical profiles of sulfate and elemental carbon aerosols, which exhibit sharp decreases from the boundary layer to the FT due to wet scavenging. The results were attributed to a large, sustained source of SOA in the FT from oxidation of long-lived volatile organic compounds. This SOA constituted the dominant component of the measured aerosol mass in the FT. In simulations of reactions forming secondary organic aerosol downwind of London Johnson et al (2006) found it necessary to increase the partitioning of organic into the aerosol phase by a factor of 500 over the partition coefficient that had been developed to simulate laboratory smog chamber studies.

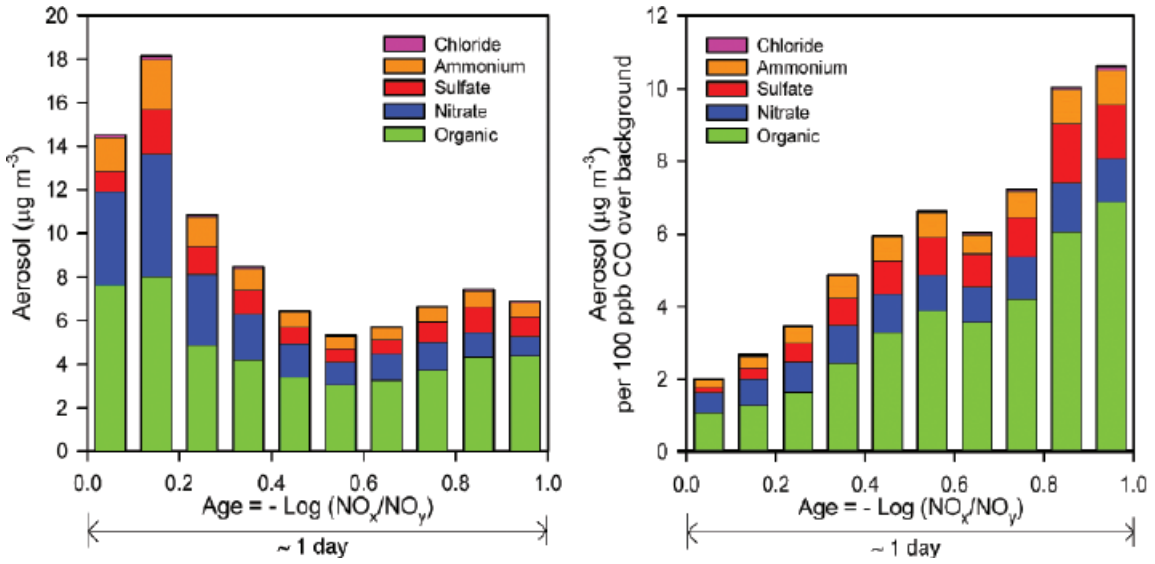


**Figure A2.3.** Measurements of the concentration of aerosol constituents by airborne aerosol mass spectrometry downwind of Mexico City, left, and normalized to excess carbon monoxide, right, to account for dilution. Measurements are binned according to photochemical age as determined from ratio of nitrogen oxides ($NO_x$ = NO + $NO_2$) to higher oxidation products of these oxides, NOy, mainly nitric acid. Modified from Kleinman et al. (2007).

Another important recent finding that may have major implications to understanding and modeling organic aerosol comes from a series of laboratory and chemical transport modeling studies that identified and quantified aerosol formation from the oxidation of isoprene (Kroll et al, 2006; Henze and Seinfeld, 2006). The atmospheric oxidation of gas-phase hydrocarbons leads to the formation of low-volatility products that partition into the condensed phase; the resulting secondary organic aerosol accounts for a substantial fraction of global organic aerosol loading and hence has an important influence on climate. Large biogenic hydrocarbons (terpenes and sesquiterpenes) have long been believed to be the primary source of SOA on a global scale; although the biogenic hydrocarbon, isoprene, the second most abundant hydrocarbon in the earth's atmosphere after methane, is emitted in much larger quantities (~500 Tg $yr^{-1}$) than the terpenes, because of its low molecular weight it has generally been believed not to form SOA in appreciable amounts. However in recent environmental chamber experiments, photooxidation of isoprene has been shown to produce SOA in small but appreciable quantities (mass yields of 1-5%). Because of the large source strength of isoprene, even these small yields imply a major SOA source missing from previous atmospheric models. Inclusion of SOA formation from isoprene in a global chemical transport model was found to more than double the predicted SOA loading. This work indicates that isoprene may be the single most important contributor to SOA on a global scale, with important implications for global climate. The availability of a model representation of this process will allow it to be incorporated into large scale chemical transport models and climate models.

**References**

**De Gouw**, J. A., et al., 2005: Budget of organic carbon in a polluted atmosphere: Results from the New England Air Quality Study in 2002, *J. Geophys. Res*., **110**, D16305, doi:10.1029/2004JD005623.

**Heald**, C. L., D. J. Jacob, R. J. Park, L. M. Russell, B. J. Huebert, J. H. Seinfeld, H. Liao, and R. J. Weber, 2005: A large organic aerosol source in the free troposphere missing from current models, *Geophys. Res. Lett.*, **32**, L18809, doi:10.1029/2005GL023831.

**Henze**, D. K. and Seinfeld, J. H., 2006: Global secondary organic aerosol from isoprene oxidation. Geophys. Res. Lett. 33, L09812, doi:10.1029/2006GL025976.

**Johnson** D., S.R. Utembe, M.E. Jenkin, R.G. Derwent, G.D. Hayman, M.R. Alfarra, H. Coe and G. McFiggans, 2006: Simulating regional scale secondary organic aerosol formation during the TORCH 2003 campaign in the southern UK, *Atmos. Chem and Phys.* **6**: 403-418.

**Kleinman**, L. I., Springston, S. R., Daum, P. H., Lee, Y.-N., Nunnermacker, L. J., Senum, G. I., Wang, J., Weinstein-Lloyd, J., Alexander, M. L., Hubbe, J., Ortega, J., Canagaratna, M. R., and Jayne, J., 2007: The time evolution of aerosol composition over the Mexico City plateau. *Atmos. Chem. Phys. Discuss*. **7**, 14461-14509.

**Kroll**, J. H., Ng, N. L., Murphy, S. M., Flagan, R. C., and Seinfeld, J. H., 2006: Secondary organic aerosol formation from isoprene photooxidation. *Environ. Sci. Technol.* **40**, 1869-1877, doi:10.1021/es0524301.

**Volkamer**, R., J. L. Jimenez, F. San Martini, K. Dzepina, Q. Zhang, D. Salcedo, L. T. Molina, D. R. Worsnop, and M. J. Molina, 2006: Secondary organic aerosol formation from anthropogenic air pollution: Rapid and higher than expected, *Geophys. Res. Lett.*, **33**, L17811, doi:10.1029/2006GL026899.

## Appendix A.3

An example of the importance of composition when parameterizing the first indirect effect is shown in **Figure A3.1**. Physical measurements, of the dependence of critical supersaturation of particles as a function of their diameter, show marked differences above and below a shallow stratus deck in the vicinity of Pt. Reyes, CA. Here the two diagonal lines (slope of -3/2 on a logarithmic plot of supersaturation vs dry diameter) indicates the dependence of critical supersaturation on particle size for constant composition according to the Köhler theory of cloud drop activation. Departure from this dependence indicates dependence on composition. The difference in critical supersaturation for two ionic substances, sodium chloride and ammonium sulfate, is about 32%, e.g., an increase from 0.2 to 0.26%, a substantial increase. Shown on the figure are measurements above and below a cloud deck off the coast of northern California. Activation of the above-cloud particles of the same size requires a greater supersaturation, and activation of particles at both altitudes requires a supersaturation about three times as high as would be expected for particles consisting entirely of inorganic salts; also shown for reference are measurements made in the eastern Caribbean, which are consistent with an inorganic salt composition. Simultaneous measurements of bulk composition show a greater organic fraction above clouds than below. Measurements of size dependent composition confirm that this organic fraction is greatest in the diameter range corresponding to the CCN measurements, 40 - 200 nm. In the absence of the chemical measurements the reasons for the differences in critical supersaturation would not be known; in the absence of the physical measurements the consequences of the differences in composition would not be known.

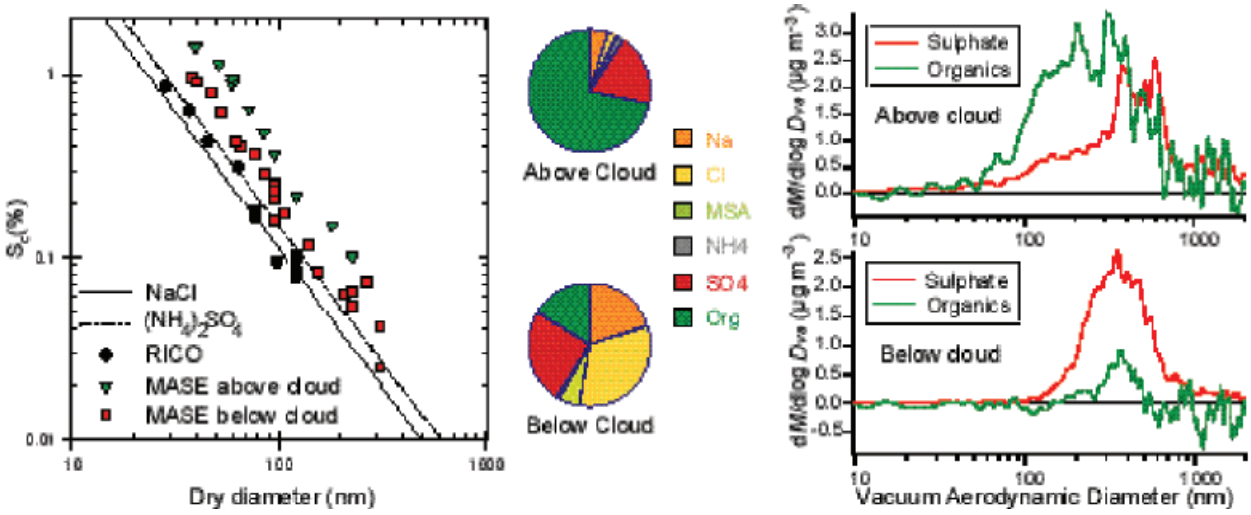


**Figure A3.1.** Example of difference in CCN activity of aerosols and relation to composition below (110-170 m) and above (400-470 m) clouds measured off the coast of California, north of San Francisco, on July 25, 2005. Left panel shows critical supersaturation as a function of particle size; also shown for comparison are measurements made in clean maritime air in the eastern Caribbean boundary layer and the theoretical dependence for two soluble salts, sodium chloride and ammonium sulfate (J. Hudson, Desert Research Institute, unpublished measurements; Hudson, 1989; Hudson and Da, 1996). Pie charts (middle panel) show ionic composition measured by PILS (particle into liquid sampler) and organic fraction inferred by difference from total volume, inferred from light scattering at low relative humidity and assumed mass scattering efficiency of 3.3 m2 $g^{-1}$; below cloud mass concentration 8.1 ± 0.3 µg $m^{-3}$; above cloud, 3.8 ± 0.2 µg $m^{-3}$ (Y.-N. Lee, Brookhaven National Laboratory, unpublished measurements). Right panel shows the distribution of sulfate and organic mass with particle size above cloud (top) and below cloud (bottom) measured by aerosol mass spectrometry (M. Alexander, Pacific Northwest National Laboratory, unpublished measurements). From Ghan and Schwartz (2007).

**References**

**Ghan** S. J., and Schwartz S. E., 2007: Aerosol Properties and Processes: A Path from Field and Laboratory Measurements to Global Climate Models. *Bull. Amer. Meteorol. Soc*. **88**, 1059–1083.

**Hudson** J. G. and Da X., 1996: Volatility and size of cloud condensation nuclei. *J. Geophys. Res.* **101**, 4435-4442.